SHARING

SELF-ORGANIZED HETEROGENEOUS ADVANCED RADIO NETWORKS GENERATION

Deliverable D3.5

Progress in RF Front-End, Antenna Design

Date of delivery	31/01/2015
Contractual date of delivery	31/01/2015
Project number	C2012/1-8
Editor(s)	Yolanda Fernández (TTI), Adrián Sánchez (TTI)
Author(s)	Yolanda Fernández (TTI), Adrián Sánchez (TTI), Sylvie Mayrargue (CEA), Cyril Jouanlanne (CEA)
Dissemination level	PU
Workpackage	3
Version	1.0
Total number of pages	42

Abstract:

This document describes the main challenges related to RF front-ends and antennas to support carrier aggregation, proposing innovative solutions which will be studied in SHARING project. On the one hand, the main design for power amplifiers to support carrier aggregation is evaluated, promoting a reconfigurable solution to provide energy savings which are assessed using a commercial product as reference in terms of energy efficiency. And on the other hand, an antenna solution using frequency agility optimized according to the different carrier aggregation modes is proposed. This approach provides a miniature highly efficient antenna solution.

Keywords: carrier aggregation, reconfigurable power amplifier, antenna, frequency agility

Document Revision History

Version	Date	Author	Summary of main changes
0.1	01/10/2014	All	Creation of the Table of Contents (ToC)
0.2	30/10/2014	TTI	TTI contribution
0.3	09/12/2014	CEA	CEA contribution
0.4	10/12/2014	TTI	Integrated version
0.8	15/12/2014	TTI & CEA	Internal review done
1.0	05/02/2015	TTI	Final version

TABLE OF CONTENTS

LIST OF FIGURES

LIST OF TABLES

EXECUTIVE SUMMARY

Deliverable D3.5 "Progress in RF front-end, antenna design" presents the analysis and results for some key aspects related to RF front-ends and antennas in order to deal with the challenging RF issues to support carrier aggregation (CA) in small cells scenarios.

WP3 activities include four tasks, this deliverable concerns task T3.4 "RF and antenna design". Innovative solutions are investigated for RF front-ends and antennas to support CA, improving energy efficiency and reducing size and/or cost. CA will play an important role in future cellular networks increasing the bandwidth up to 100MHz and providing flexibility for using the available spectrum. Two different aspects are studied: reconfigurable power amplifiers (PA) capable to adapt to different CA modes and providing energy savings; and miniaturized reconfigurable antennas using frequency agility to optimize antenna radiation patterns.

Different key aspects related to RF front-ends and especially power amplifiers to support carrier aggregation were evaluated. A unique reconfigurable power amplifier is proposed for various component carriers (CCs) to be implemented in small cell scenarios for which it is necessary to reduce the size and the cost.

Base station transmitter specifications were reviewed to identify PA requirements. Furthermore, different test models to evaluate the technical specifications were also identified. Several simulations were done to define PA requirements according to the number of CCs for intra-band contiguous CA. For each CA configuration, the required output back-off (OBO) level was determined on the basis of an analysis of the peak-to-average power ratio (PAPR) and the adjacent channel leakage ratio (ACLR). A commercial PA was selected to assess the proposed reconfigurable solution in terms of energy efficiency. Evaluation results show that, in terms of energy efficiency, there is no improvement compared to a conventional PA in case of 5 contiguous CCs. However, in case of less contiguous CCs, results clearly show improvements in terms of relative power added efficiency (PAE) that can be awarded to the reconfigurability capabilities of the PA prototype. Please note that, in order to provide the energy savings, each CA configuration may correspond to different PA operating points. This study will be extended to intra-band non-contiguous CA.

SHARING addresses the issue of dense deployment of small cells operating in LTE bands 7 and 20. In this case, base stations are located in an urban environment, thus, a high level of integration and some miniaturization of the whole system especially of the antennas is required. This should not result in performance degradation and if so, this degradation should be minimized as much as possible.

The size of an antenna is directly linked to several parameters such as its operating frequency, its efficiency and its bandwidth. In order to reduce the size of an antenna, an action is required on (at least one of) these parameters. Given the operating frequencies, only band 20 antenna components require miniaturization. Taking into consideration that, in the considered CA scenarios, only one pair of channels (UL and DL) is used at the same time in band 20, the required instantaneous bandwidth can be reduced. This is achieved through the use of frequency agility leading to a miniaturization of band 20 antenna components without impacting the performance of the whole system.

A size optimized complex antenna system covering both bands 7 and 20 has been designed and simulated using a 3D electromagnetic simulation software. This antenna system has similar performance in terms of efficiency than regular base station antennas but is better optimized in terms of integration and size.
Based on aforementioned simulation results, several prototypes will be built and experimentally characterized in the next phase of the project.

1   INTRODUCTION

This report presents some key aspects related to RF front-ends and antennas to support CA, proposing innovative solutions which have been evaluated showing some intermediate results. As a reminder, WP3 activities are divided into four tasks and this deliverable applies to T3.4 "RF and antenna design".

In chapter 2, different key aspects related to RF front-ends and especially PAs to support CA were evaluated. A unique reconfigurable power amplifier is proposed to be implemented in small cell transmitter architecture capable to adapt to different CA modes providing energy savings versus a conventional power amplifier. In small cell scenarios, it is reasonable to use a unique PA for various CCs to reduce the size and the cost because the power levels that PA handles are not strongly challenging as in macro cell scenarios. In macro cell scenarios, a PA is normally used per CC due to the power level that the PA handles.

Base station transmitter specifications were reviewed to assess PA requirements to fulfil 3GPP specifications. Furthermore, different test models to evaluate the technical specifications were presented identifying which test model is used for each transmitter specification.

Power amplifier requirements were studied based on CCDF (PAPR) and ACLR evaluation depending on the number of CCs, defining the required OBO level in each CA configuration. And finally, a commercial power amplifier was selected to assess the proposed reconfigurable solution in terms of energy efficiency.

In chapter 3 an antenna system has been developed and optimized for this specific RF front end and CA available configurations. The different antenna concepts and techniques such as frequency agility are explained in detail through simple simulation setups. Then, a detailed evaluation of the complete antenna system is made using electromagnetic simulation software.

2   RECONFIGURABLE RF FRONT-END TO SUPPORT CARRIER AGGREGATION

2.1 Introduction

Corresponding scenario in D2.2: 2.7.1"Carrier aggregation using reconfigurable RF front-ends"

One of the key features of LTE-Advanced (LTE-A) is to extend up to 100 MHz of bandwidth reaching 1 Gbps peak data rate for low mobility applications and 100 Mbps for high mobility. This feature is coined carrier aggregation (CA) because up to 5 component carriers (CC) could be aggregated improving network efficiency and user performance by dynamically allocating traffic across the entire available spectrum. Currently, only 3 CCs are allowed following 3GPP specifications [1].Beyond this case, the scope of this study is to evaluate the performance of RF front-end dealing with up to 5 CCs.

There are different modes of CA depending on the way that CCs are allocated in the spectrum. If CCs are allocated in the same frequency band, it is defined as intra-band CA; and if CCs are allocated in different frequency bands, inter-band CA. Furthermore, intra-band contiguous CA is implemented when CCs are allocated contiguously into the same frequency band and intra-band non-contiguous CA is implemented when CCs are allocated separately into the same frequency band.

a)   b)

c)
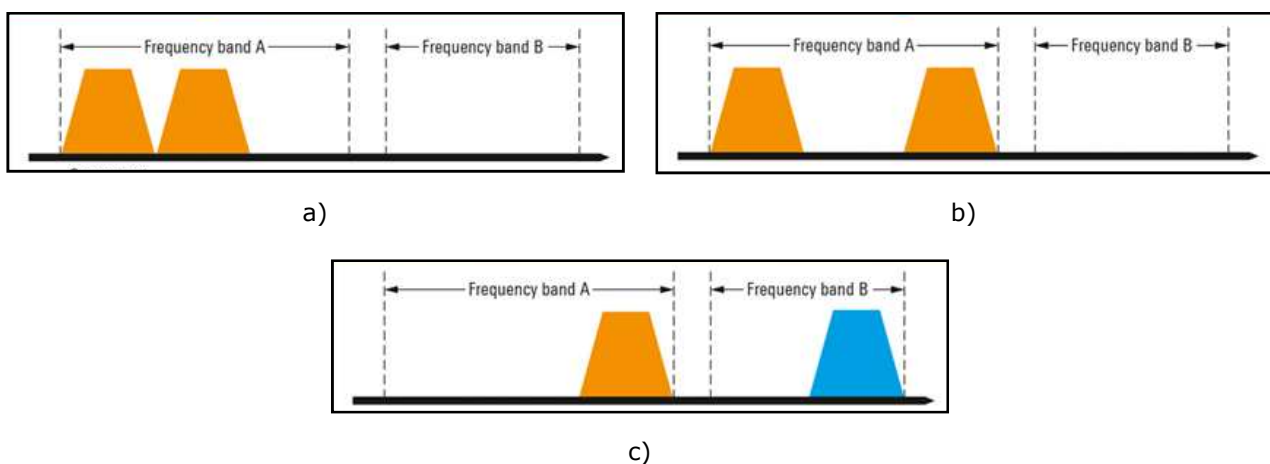
Figure 1   Different CA modes: a) Intra-band contiguous, b) Intra-band non-contiguous and c) Inter-band

Figure 1 represents the occupied spectrum of each CA mode. The allowed channel bandwidths for each CC are 1.4 MHz, 3 MHz, 5 MHz, 10 MHz, 15 MHz or 20 MHz. Presently, the maximum aggregated bandwidth is 60 MHz[1].

LTE-A is defined to operate in certain frequency bands depending on the use of FDD or TDD. In Europe, the operating bands for FDD are bands 1, 3, 7, 8 and 20, while bands 33, 34, 38 and 40 are available for TDD. This study is focused on FDD, and band 7 and band 20 were selected for the evaluation to be in line with the hardware demonstrator that will be developed into WP7.

To support CA and its bandwidth flexibility, RF front-ends should fulfil certain characteristics because RF components have to work in larger bandwidth. Inside RF front-end, the power amplifier (PA) is one of the most power consuming components and it demands high linearity requirements due to LTE-A signals features. Typical peak-to-average-power ratio (PAPR) for LTE-A signals could be estimated around 8-10dB for each CC. These systems require PAs with superior performance, requiring large output back-off (OBO) power levels to avoid spectral spreading. To meet these stringent linearity requirements and at the same time operating the amplifiers at their highest possible efficiency becomes a challenging issue.

The scope of this study is to evaluate a reconfigurable PA capable of adapting to different CA modes from an energy efficiency perspective. A conventional amplifier works usually with a fixed operating point, while the proposed solution will modify the operating point to adjust to different CA modes. Depending on the number of carriers handled and the CA mode, the PA requirements are different. Therefore, the study will define the best operating point for each CA mode to provide energy savings compared to a conventional PA.

The study refers to the base station (BS) case because it could present higher tunability demand, and the scenario will be that of a small cell. In typical macro cell scenarios, a PA is used per CC in transmitter architecture as shown in Figure 2 a), because the power level that PA handles is high and

the PAis optimized for narrowband performance. However in small cell scenarios, it is reasonable to use a unique PA for various CCs to reduce the size and the cost because the power levels that PA handles are not strongly challenging as in macro cell scenarios (Figure 2 b).

a)   b)

Figure 2   Transmitter architecture for CA: a) using a PA per CC and b) using a unique PA for various CCs

The study consists in evaluating the PA performance when a unique PA is implemented for CA in small cell scenarios. The target is to e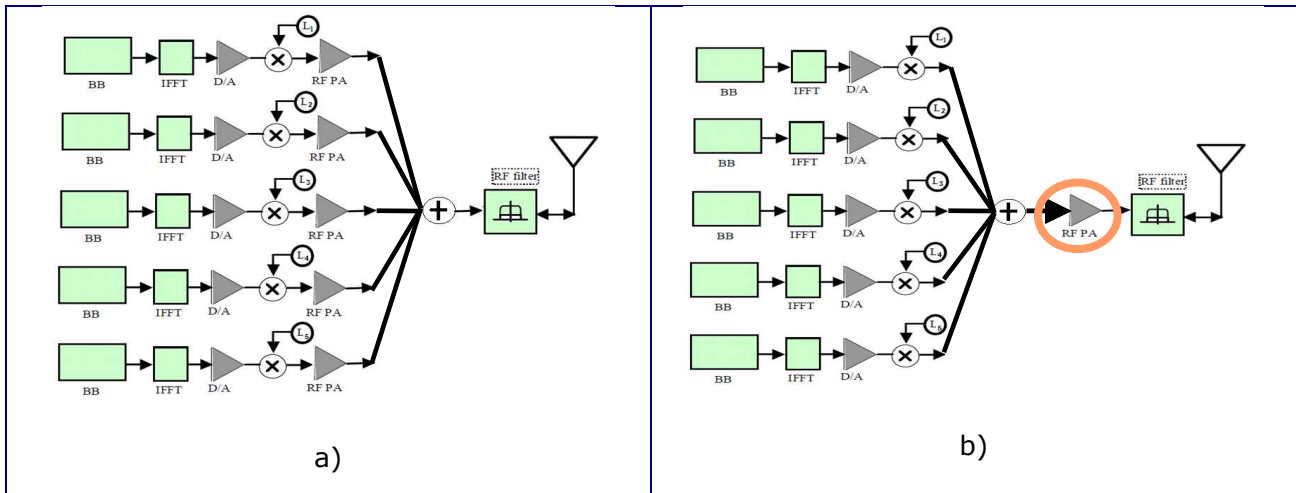valuate its performance versus the number of CCs for CA and CA modes to check whether 3GPP specifications in terms of PA linearity and intermodulation constraints are fulfilled, and at the same time calculate energy savings through PA reconfigurability. In the next section, eNB transmitter specifications are discussed to take into account the PA requirements.

2.2 eNB transmitter specifications

Concerning PA design, unwanted emissions are the most important parameters to take into account during the design process. Unwanted emissions consist of out-of-band emissions and spurious emissions. Out-of-band emissions are very close to the channel bandwidth resulting from the modulation process and non-linearity in the transmitter, closely related to PA performance. The power that leaks from a transmitted signal into adjacent channels can interfere with transmissions in the neighbouring channels and impair system performance. On the other hand, spurious emissions are emissions which are caused by unwanted transmitter effects such as harmonics emission, parasitic emission, intermodulation products and frequency conversion products, but exclude out of band emissions.

Some out-of-band emissions requirements for the BS transmitter are specified in terms of Adjacent Channel Leakage power Ratio (ACLR) and operating band unwanted emissions. The ACLR parameter verifies that system transmitters are performing within specified limits. The ACLR requirement constrained by 3GPP standard is defined to be at least 45 dB [2]. This parameter is one of the most significant for PA design because the ACLR is frequently dominated by the 3rd-order intermodulation distortion (IMD3) of the device. A convenient way to look at the source of ACLR degradation in an RF device is to model the wideband carrier spectrum as a collection of individual CW subcarriers. Each of these subcarriers would carry a fraction of the total carrier power. The ACLR performance of multiple wideband carriers looks much like the ACLR where each individual wideband carrier occupies a fraction of the total wideband carrier bandwidth. The ACLR for a carrier adjacent to the last carrier in the contiguous collection of wideband carriers rides on the high shoulders of the IMD3-induced distortion response. This causes the ACLR for a multicarrier case to be considerably worse than that for a single-carrier system.

For eNB transmitter, different test models [3] have been defined in order to evaluate the technical specifications which should be fulfilled. These test models and the evaluated specifications are summarized in Table 1.

Table 1 eNB conformance tests at transmitter [3]

Transmitter characteristics (Section 6 3GPP TS 36.141)	
Test models type	**Test model use case**
E-UTRA test model 1.1	BS Output power Unwanted emissions - Occupied bandwidth - ACLR - Operating band unwanted emissions - Transmitter spurious emissions Transmitter intermodulation RS absolute accuracy
E-UTRA test model 1.2	ACLR Operating band unwanted emissions
E-UTRA test model 2	Total power dynamic range EVM of single 64QAM PRB allocation Frequency error
E-UTRA test model 3.1	Output power dynamics - Total power dynamic range Transmitted signal quality - Frequency error - EVM for 64QAM
E-UTRA test model 3.2	Transmitted signal quality - Frequency error - EVM for 16QAM
E-UTRA test model 3.3	Transmitted signal quality - Frequency error - EVM for QPSK

This study is focused on the PA performance, therefore E-UTRA test model 1.1 (E-TM1.1) was selected for simulations because it verifies almost all specifications related to PA. In E-TM1.1 test model, all PDSCH resource blocks have the same power. Further studies will also evaluate E-TM1.2 because it simulates multiple users whose devices are operating at different power levels. This scenario results in a higher crest factor, which makes it more difficult to amplify the signal without creating additional unwanted spectral content.

2.3 PA requirements evaluation

2.3.1   PA requirements evaluating CCDF (PAPR)

LTE-A signals do not have a constant envelope signal and any non-linear amplifier generates various forms of distortion. The simplest form of distortion occurs when a signal (envelope) causes a device to generate non-linear distortion products. Assuming a memory less non-linear system i.e., a non-linear system that produces distortions corresponding to the instantaneous value of the signal, the impact of these instantaneous distortions depends on the statistical probability of their occurrences.

The Complementary Cumulative Distribution Function (CCDF) characterizes the weighted probability of the signal excursions (peak-amplitude distributions relative to the envelope average) that lead to the distortions, by indicating the number of samples where the signal peak power exceeds its average power by a certain value. PAPR statistics are given in terms of the CCDF. The CCDF shows the probability of an OFDM frame exceeding a given PAPR,

$$CCDF\big(PAPR(x)\big) = Pr(PAPR(x) > PAPR_0)$$

To calculate the PA Back-Off (BO), it is normally sufficient to use the 0.01% CCDF (PAPR) of the composite waveform.

Different CCDF (PAPR) simulations were run using E-TM1.1 for single CC with different bandwidths (Figure 3).
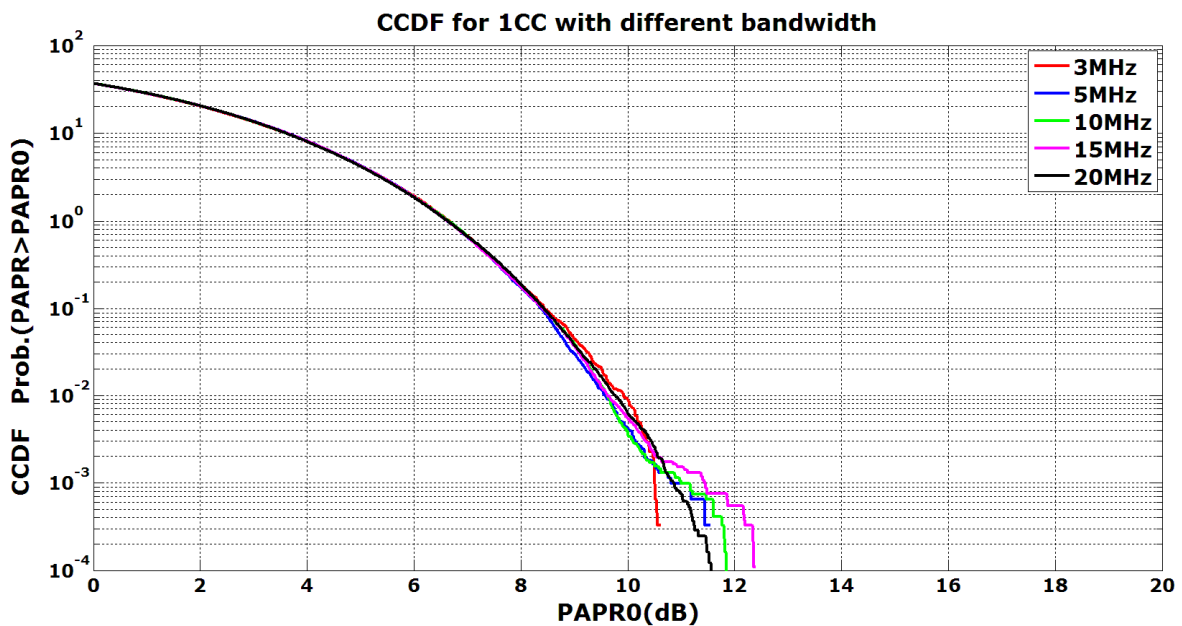
Figure 3   CCDF (PAPR) plot for 1CC with different bandwidth (using E-TM1.1)

CCDF (PAPR) results at 0.01% probability are 9.6 dB for 5MHz, 10MHz and 15MHz, 9.7 dB for 20MHz and 9.9dB for 3MHz.Therefore during the PA design, it should be taken into account that at least 9.6 dB Output Back-Off (OBO)is required to support single CC with 5MHz, 10 MHz or 15MHz. Apart from CCDF (PAPR) simulations, ACLR simulations were done to complement the PA requirements evaluation. They are presented in the next section.

To be able to implement CA in a unique PA, CCDF (PAPR) simulations were done for different numbers of CCs, up to 5 for intra-band contiguous CA mode, to evaluate the PA OBO requirements, testing different bandwidths. For 2 contiguous CCs, CCDF results at 0.01% probability are 11.8 dB for 5MHz, 10MHz, 15MHz and 20MHz, and 12 dB for 3MHz as shows Figure 4. In this CA mode, the PA should be designed with at least 11.8 dB OBO for 5MHz, 10 MHz, 15 MHz and 20 MHz.

CCDF for 2CCs with different bandwidth
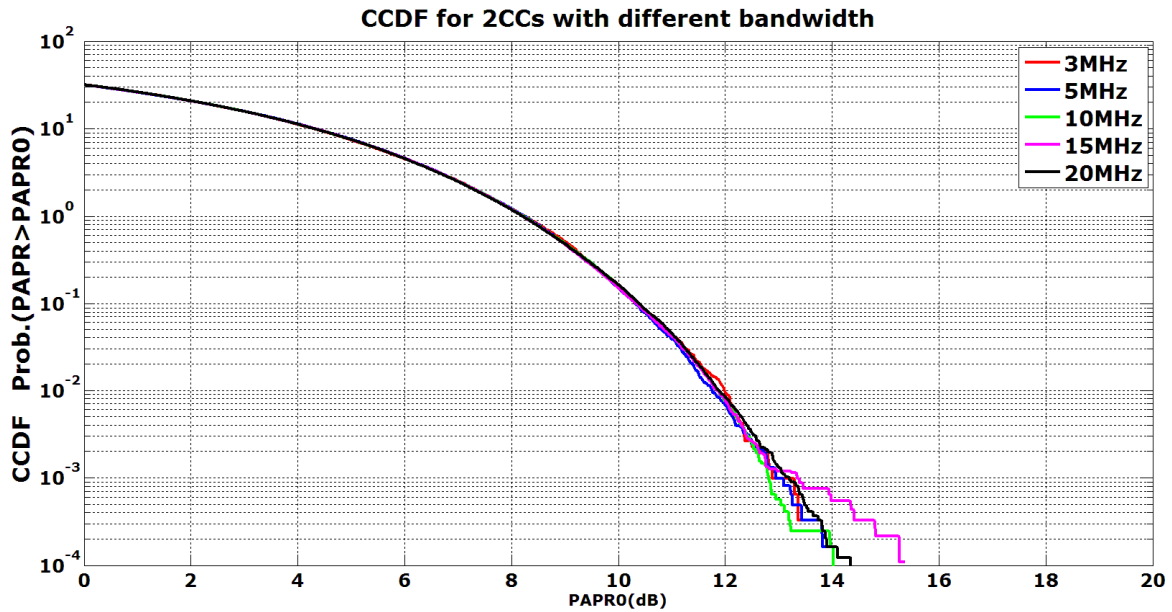
Figure 4   CCDF (PAPR) plot for 2CCs with different bandwidth (using E-TM1.1)

For 3 contiguous CCs, CCDF (PAPR) results at 0.01% probability are 13.3 dB for 5MHz, and 13.4 dB for 3MHz, 10MHz, 15MHz and 20MHz as shows Figure 5.

CCDF for 3CCs with different bandwidth
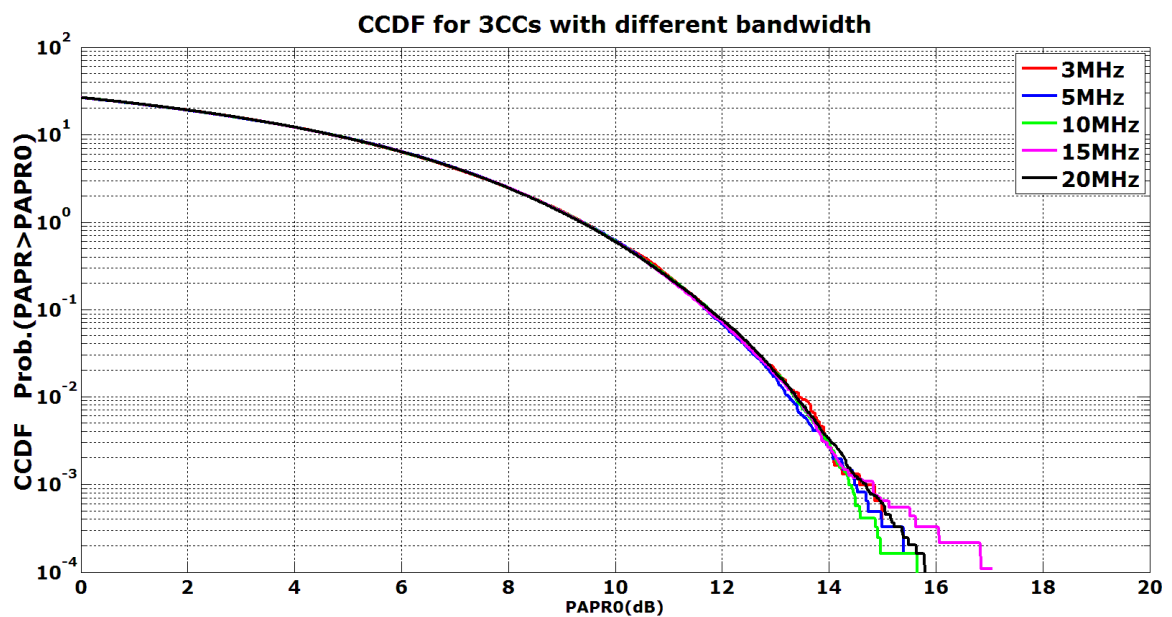
Figure 5   CCDF (PAPR) plot for 3CCs with different bandwidth (using E-TM1.1)

For 4 contiguous CCs, CCDF (PAPR) results at 0.01% probability are 14.3 dB for 5MHz, 14.4 dB for 10MHz, 15MHz and 20MHz, and 14.5 dB for 3MHz as shows Figure 6.
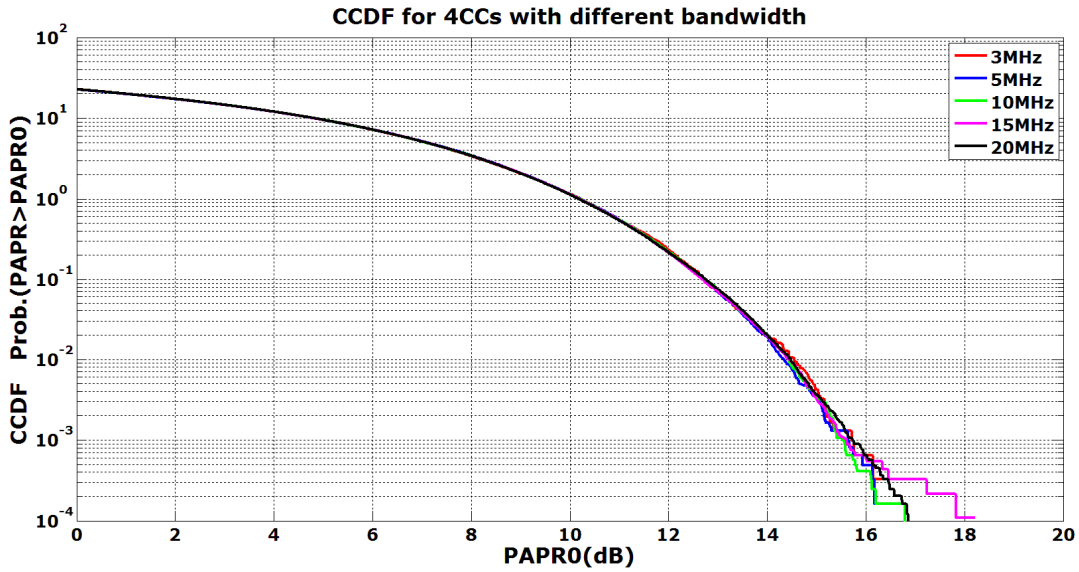
Figure 6   CCDF (PAPR) plot for 4CCs with different bandwidth (using E-TM1.1)

Finally for 5 contiguous CCs, CCDF (PAPR) results at 0.01% probability are 15.2 dB for 5MHz, and 15.3 dB for 3MHz, 10MHz, 15MHz and 20MHz as shows Figure 7.
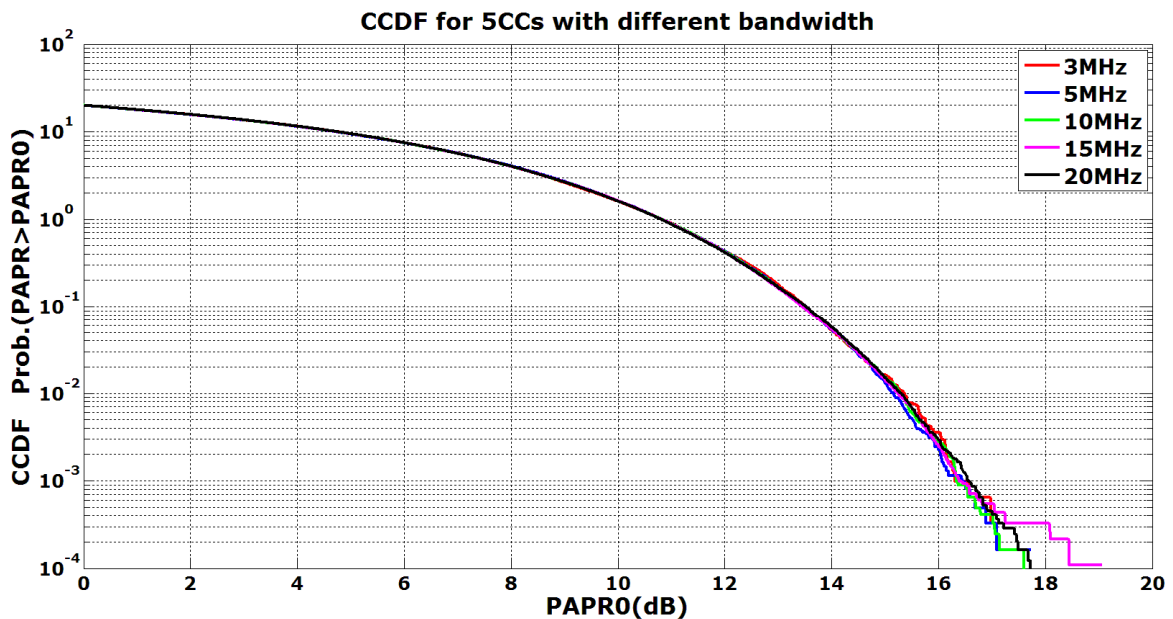
Figure 7   CCDF (PAPR) plot for 5CCs with different bandwidth (using E-TM1.1)

Figure 8 summarizes CCDF (PAPR) results for different number of CCs and different bandwidth. It is clearly observed that the typical 0.01% CCDF (PAPR) value used to calculate the PA OBO increases with the number of CCs, but keeps almost constant through the different CC bandwidths. Consequently a reconfigurable PA capable to work with up to 5 CCs presents higher linearity constraints than with a lower number of CCs.
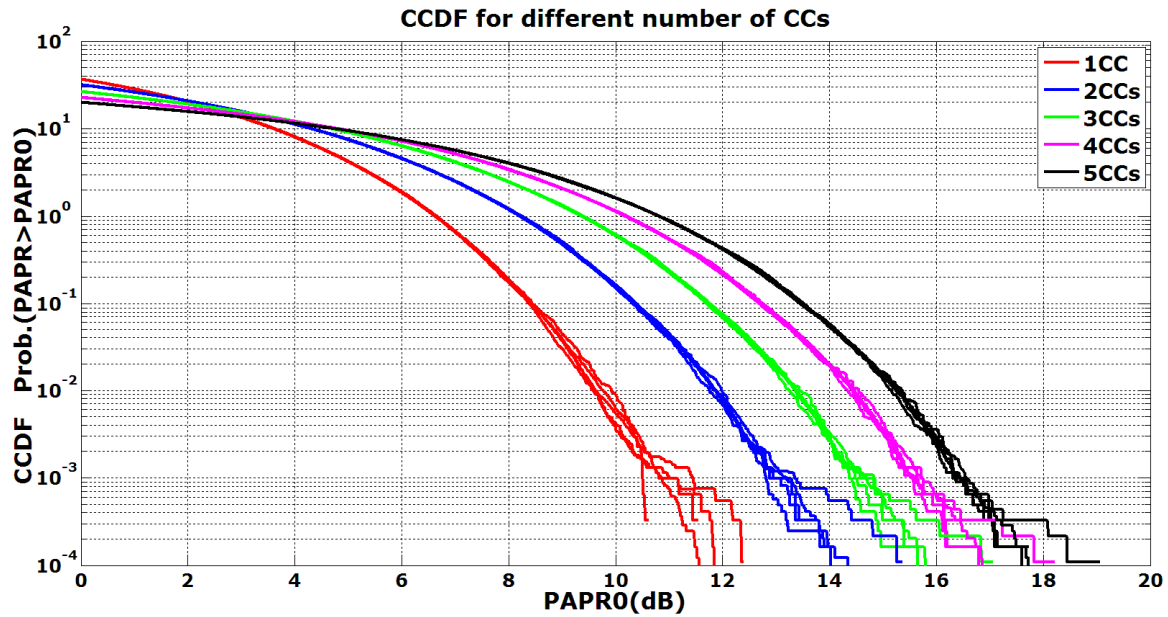
Figure 8   CCDF (PAPR) plot for different number of CCs and bandwidth (using E-TM1.1)

Table 2summarizes 0.01% CCDF (PAPR) results for different number of CCs with 5MHz bandwidth using test model E-TM1.1.

Table 20.01% CCDF (PAPR) results for different number of CCs with 5MHz bandwidth (using E-TM1.1)

Number of CCs	0.01% CCDF (PAPR)
1	9.6 dB
2	11.8 dB
3	13.3 dB
4	14.3 dB
5	15.2 dB

These values are normally sufficient to calculate the PA OBO in case of single CC. However ACLR requirements were also evaluated depending on the number of CCs to complement CCDF (PAPR) simulations. Next section presents ACLR simulations results.

2.3.2 PA requirements evaluating ACLR

ACLR is a measure of the nonlinear characteristics of a device under test, in this case the PA and indicates the amount of spectral regrowth occurring in adjacent channels. This evaluation complements the CCDF (PAPR) evaluation which is focused on in-band channel.

Test models E-TM1.1 and E-TM1.2 are used to evaluate ACLR specifications at transmitter architecture. Several simulations were performed using E-TM1.1 to evaluate the impact of PA OBO over ACLR results depending on the number of CCs in intra-band contiguous CA. During the simulations, a PA model was used modifying only 1dB output compression power without introducing constraints as noise figure, saturation power, etc to shorten simulations.
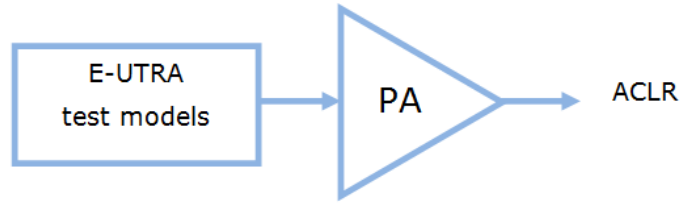
Figure 9   Block diagram of ACLR simulations

Figure 10 presents ACLR results versus PA OBO for different number of CCs using the test model E-TM1.1. All CCs in these simulations have 5 MHz bandwidth. Anyway similar results are obtained with different bandwidths.
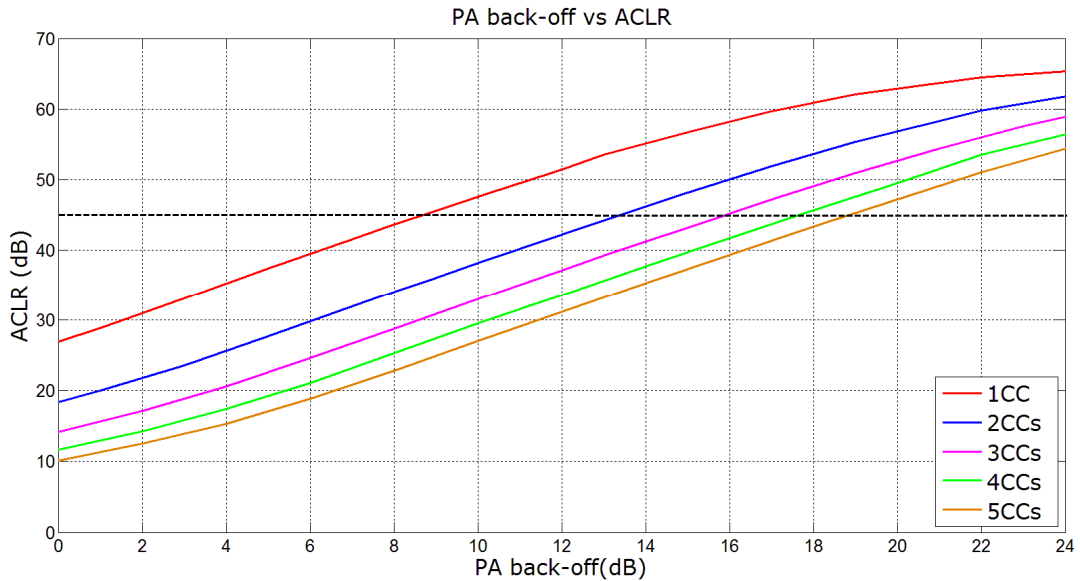
Figure 10   ACLR results versus PA back-off for different number of CCs (using E-TM1.1)

According to 3GPP specifications, ACLR requirement should be at least 45 dB. Table 3 summarizes the PA OBO to reach 45 dB ACLR for different number of contiguous CCs. These values should be evaluated together with CCDF (PAPR) results to define the PA requirements.

Table 3 PA OBO requirement to obtain 45 dB ACLR for different number of CCs

Number of CCs	PA OBO (ACLR = 45 dB)
1	8.7 dB
2	13.4 dB
3	15.9 dB
4	17.7 dB
5	18.9 dB

Some simulations results are depicted in Figure 11, Figure 12 and Figure 13 showing output spectrum for 5 contiguous CCs with 10 MHz bandwidth with different 1dB compression output power level at PA to assess ACLR results. Figure 11 shows the output spectrum fulfilling ACLR specifications, with the PA working with 19 dB OBO. This CA mode with 5 CCs is the most demanding in terms of linearity for the reconfigurable PA design.
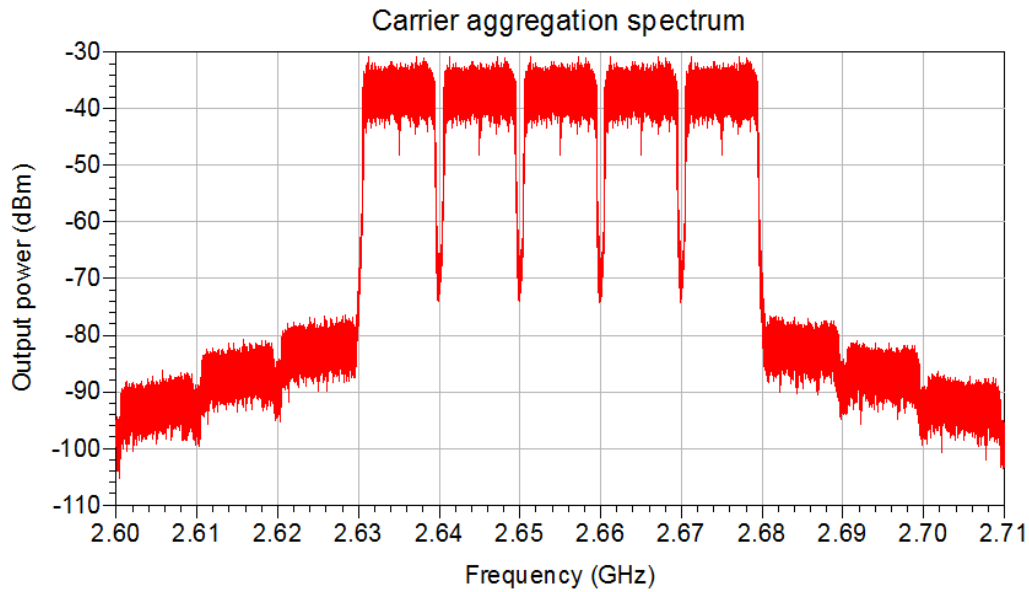
Figure 11   Output spectrum for 5 contiguous CCs with 10MHz bandwidth reaching 45 dB ACLR(OBO = 19dB)

Figure 12 shows the output spectrum for 5 contiguous CCs with 10 MHz bandwidth reaching 54 dB ACLR, because in this case the PA is configured with 24dB OBO. Comparing Figure 11 and Figure 12, it is clearly observed that the adjacent channel in Figure 11 has higher level and higher variability. On the other hand, if the PA is configured as in Figure 12with OBO level higher than the required one, the energy efficiency at PA will be reduced due to PA features.
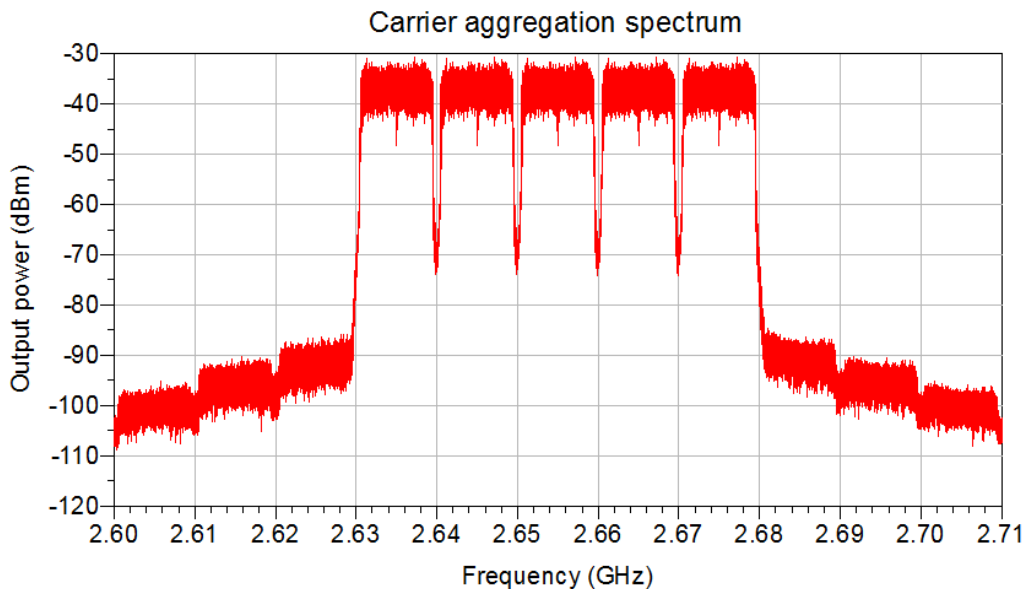
Figure 12   Output spectrum for 5 contiguous CCs with 10MHz bandwidth reaching 54 dB ACLR (OBO = 24 dB)

Meanwhile in Figure 13, ACLR specifications are not fulfilled because the OBO level at PA is 14 dB which is not as much as necessary.
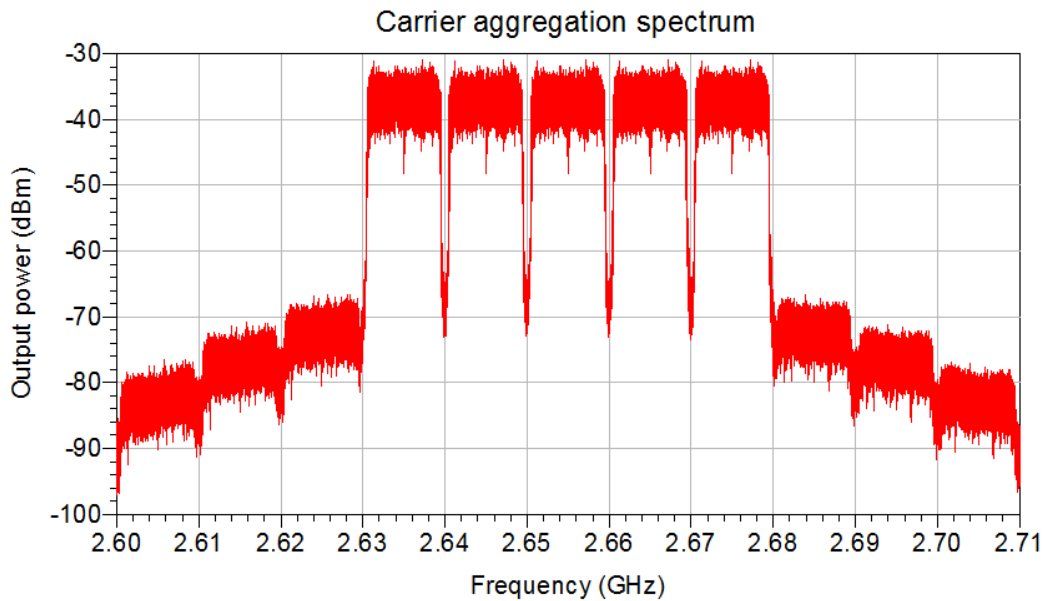
Figure 13   Output spectrum for 5 contiguous CCs with 10MHz bandwidth reaching 35 dB ACLR (OBO = 14dB)

The target is to configure the PA with the minimum OBO able to provide 45 dB ACLR and, at the same time to obtain the highest energy efficiency. Energy efficiency decreases with the OBO level, so a trade-off between ACLR and energy efficiency should be set up. The reconfigurable PA is a promising solution to cope with different number of contiguous CCs.

2.3.3   Conclusions

In this section, CCDF (PAPR) and ACLR evaluations are merged to define the PA requirements in order to develop a reconfigurable PA capable of working with up to 5 CCs optimizing energy efficiency. Table 4 shows 0.01% CCDF (PAPR) results and PA OBO level to reach 45 dB ACLR depending on the number of contiguous CCs.

Table 4 PA OBO requirements evaluating 0.01% CCDF (PAPR)and ACLR for different number of CCs (using E-TM1.1)

Number of CCs	0.01% CCDF (PAPR)	PA OBO (ACLR = 45 dB)	Total PA OBO
1	9.6 dB	8.7 dB	9.6 dB
2	11.8 dB	13.4 dB	13.4 dB
3	13.3 dB	15.9 dB	15.9 dB
4	14.3 dB	17.7 dB	17.7 dB
5	15.2 dB	18.9 dB	18.9 dB

ACLR requirement is more stringent than 0.01% CCDF (PAPR) parameter in all cases except for single CC. Therefore a reconfigurable PA should take into account 9.6 dB OBO level for 1 CC, 13.4 dB for 2 CCs, 15.9 dB for 3 CCs, 17.7 dB for 4 CCs and 18.9 dB for 5 CCs. The solution proposes reconfigurable operating points at PA to optimize energy efficiency depending on the number of CCs.

2.4 Energy efficiency enhancements provided by reconfigurable PA supporting intra-band contiguous CA

In this section, a commercial PA was selected to evaluate the proposed solution. The selected power amplifier was AFT20S015N from Freescale which will be implemented in WP7 demonstrator. Different operating points could be applied at PA providing energy savings versus a conventional PA. Freescale provides a non-linear model for this component and simulations of different operating points were performed to examine energy efficiency at each operating point. Figure 14 presents DC performance for different operating points.
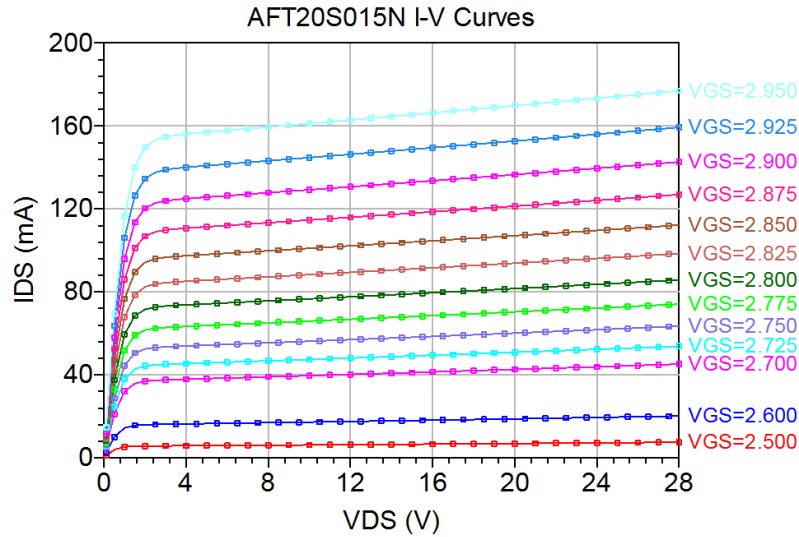
Figure 14   DC performance for different operating points in AFT20S015N

Drain voltage (VDS) and gate voltage (VGS) could be modified at PA providing different results in terms of gain, energy efficiency, etc. The recommended operating point by manufacturer is 28V drain voltage and 130 mA drain current (IDS). In the current study, the drain voltage was modified from 28 V to 8 V, without varying the gate voltage.

Figure 15 presents the power added efficiency (PAE) performance modifying the drain voltage from 28 V to 8 V with a step of 4 V. PA OBO requirement increases with the number of CCs as it was discussed in previous section. PA design should fulfil the most stringent requirements which are presented for 5 CCs, with the highest OBO level and due to that the maximum peak output power. However if lower number of CCs are supported, lower PA OBO level is required. Then for the same average output power, the required maximum output power will be lower too. In these configurations, another operating point could be configured at PA providing energy savings, while requirements are fulfilled.
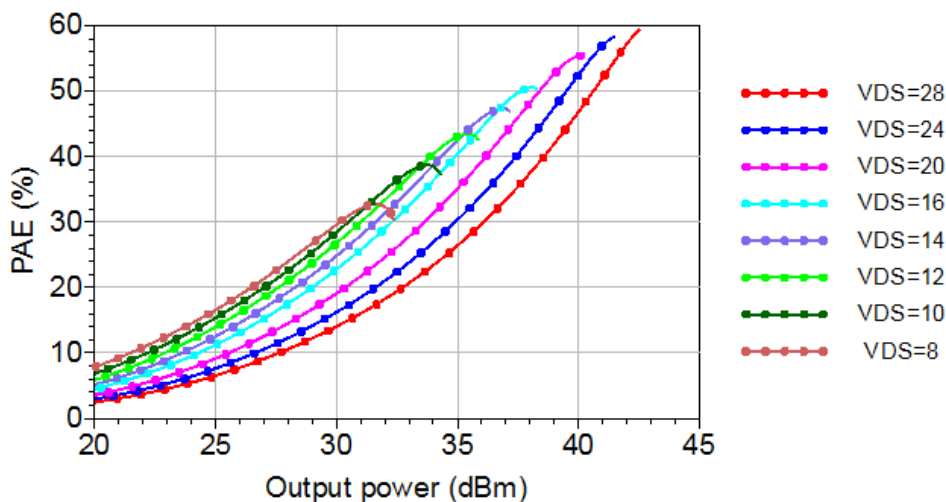
Figure 15   PAE performance for different operating points in AFT20S015N

Figure 16   Power gain versus output power performance for different operating points in AFT20S015N

The target is to define the operating point depending on the number of CCs which provides the highest energy efficiency. Based on analysis from CCDF (PAPR) and ACLR evaluation, the minimum PA OBO level depending on the number of CCs to fulfil 3GPP specifications is summarized in Table 4.

AFT20S015NR1 provides a maximum peak output power of 41.5 dBm operating at 28 V drain voltage. The reconfigurable PA should present at least 18.9 dB OBO level to support 5 contiguous CCs. Therefore the average output power could be assu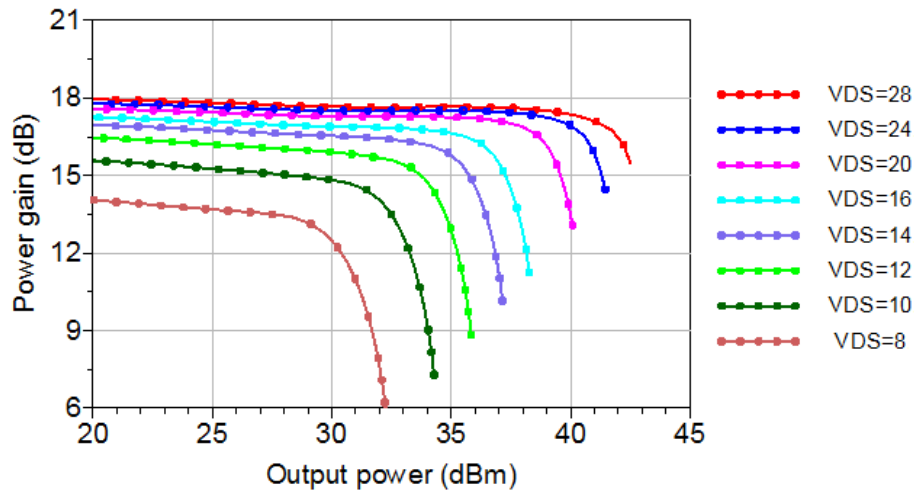med to be around22dBmconsidering a small cell scenario for this evaluation. Fixing 22 dBm average output power, AFT20S015NR1 performance was evaluated at different operating points:

Table 5 AFT20S015NR1 performance at different operating points providing 22 dBm average output power

Operating point Drain voltage (V)	Peak output power (dBm)	PAE (%) at peak output power	OBO level for 22 dBm average output power	PAE (%) at 22dBm average output power
28 V	41.5 dBm	56.5 %	19.5 dB	3.7 %
24 V	40.3 dBm	53.4 %	18.3 dB	4.5 %
20 V	38.6 dBm	50.8 %	16.6 dB	5.3 %
16 V	36.2 dBm	45.4 %	14.2 dB	6.8 %
12 V	32.5 dBm	35.3 %	10.5 dB	8.8 %
8 V	29.1 dBm	27.1 %	7.1 dB	10.7 %

Combining Table 4 and Table 5, some operating points could be assigned according to the number of contiguous CCs to provide energy savings. A conventional PA works at fixed operating point which is the one with more stringent requirements, in this case 5 contiguous CCs. For this case, the reconfigurable PA won't provide any improvement compared to the conventional one. On the other hand, if the number of CCs is reduced, the PA OBO level requirements are also reduced and additional operating points could improve energy efficiency. Table 6 summarizes relative PAE improvement using specific operating points for each intra-band contiguous CA configuration in AFT20S015NR1.

Table 6 Operating point assignment according to the number of contiguous CCs

Number of CCs	PA OBO level requirement (dB)	Operating point Drain voltage (V)	PAE (%) at 22dBm average output power	PAE improvement (%)
1	9.6 dB	12 V	8.8 %	57.9 %
2	13.4 dB	16 V	6.8 %	45.6 %
3	15.9 dB	20 V	5.3 %	30.2 %
4	17.7 dB	24 V	4.5 %	17.7 %
5	18.9 dB	28 V	3.7 %	0 %

2.5 Conclusions

In this section, a complete PA requirements evaluation depending on the number of CCs for intra-band contiguous CA has been done. The evaluation has focused on CCDF (PAPR) and ACLR parameters, defining the required OBO for each intra-band contiguous CA configuration.

A reconfigurable PA was proposed as a promising solution versus a conventional PA applying a different operating point depending on the PA requirements in each case to provide energy savings. A commercial PA was simulated to assess the proposed solution in terms of energy efficiency. In case of 5 CCs for intra-band contiguous CA, there is not any improvement versus a conventional amplifier, because it wouldn't modify the operating point. However the evaluation on the commercial PA shows 17.7% relative PAE improvement for 4 CCs, 30.2% for 3 CCs, 45.6% for 2 CCs and 57.9% for single CC. These relative PAE improvement values are related to this specific commercial PA, but they show clearly PAE improvement using different operating points at PA which are optimized for each CA mode.

The study will be extended to intra-band non-contiguous CA evaluating different number of CCs and different gaps among CCs.

3   DESIGN OF MINIATURE MULTI-BAND FREQUENCY AGILE ANTENNA SYSTEM FOR CARRIER AGGREGATION

In this chapter, an antenna system covering both LTE bands 7 and 20 is presented. A solution with two distinct antenna accesses has been designed in order to be compatible with the RF module designed by TTI (Section2). The first access will be connecting the RF chip to band 7 antenna while the other one will connect the RF chip to band 20 antenna.

Table 7 Antenna requirements

	Band 7	Band 20
Fmin	2500MHz	791MHz
Fmax	2690MHz	862MHz
Instantaneous bandwidth	190MHz	2x10MHz
Gain	>8dBi (main beam toward Z^+)	>4dBi (main beam toward Z^+)
Reference Impedance	50Ω	50Ω
Return Loss	<-10dB	
Isolation within bands	>15dB	
PCB (ground plane) dimensions	100x100 mm²	
Antenna height	30mm	

Table 7shows the requirements for both antennas. These requirements will ensure a high quality of the radio link (user experience) as well as high level of integration allowing a low profile design of the small cell base station.
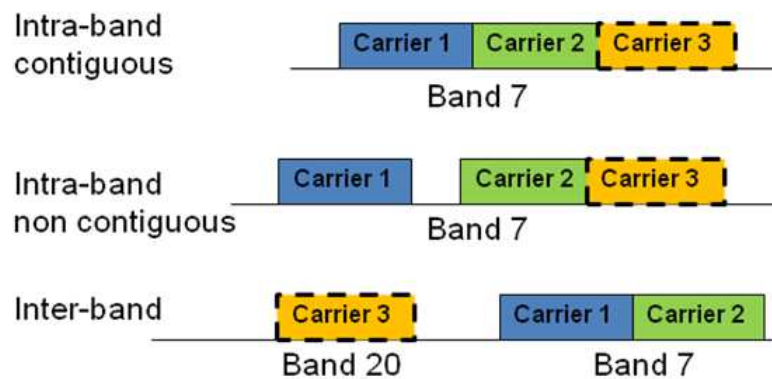
Figure 17   Possible Carrier Aggregation configurations

Table 8 Band 20 Rx and Tx channel frequencies

	Tx	Rx
State 1	791–801MHz	832–842MHz
State 2	801–811MHz	842–852MHz
State 3	811–821MHz	852–862MHz

Table 8gives an overview of the frequency bands that should be covered by each state of the frequency agile antenna.

The Carrier Aggregation (CA) configuration requires band 7 to be completely covered simultaneously while it only requires one channel of the band 20 to be covered at a time. The design of the antenna system has taken this configuration as an opportunity to introduce frequency agility in the design of the band 20 antenna. Therefore, only one Tx and the corresponding Rx channel (Table 8andFigure 18) will be covered at a time. Such a design will then require covering less instantaneous bandwidth than a passive antenna. Together with some other features, this design will allow the miniaturization of band 20 antenna without compromising its performance. Of course, the design will be more challenging and will require some active components.

The available antenna volume does not require band 7 antenna to be miniaturized. Therefore, a simple patch antenna has been selected because such an antenna easily fulfills all the wished requirements in this band.

These two antennas will also have to work together and simultaneously on the same PCB without perturbing and impacting each other. Therefore, coupling issues as well as radiation perturbation will be taken into account during the design of the antenna system. It will be difficult to avoid completely any perturbation or impact from one antenna onto the other but a specific work will be performed to reduce them enough so that both antennas work well together on the same PCB.

In this chapter, a complete antenna solution fulfilling all the antenna requirements will be presented. Each antenna will be first presented as a stand-alone antenna concept to understand how it operates. The combined solution will be then presented showing the performance of the whole antenna system.

The developments works have been carried out using 3D electromagnetics simulation tools. Only simulated results are described in this document to illustrate the results of concept investigations.

3.1 Band 20 frequency agile antenna

LTE band 20 is divided in 3 different channels that consist of one Tx and one Rx sub-channels both 10MHz wide (Figure 18). Those sub-channels are only 40MHz away from each other. The band 20 antenna will thus have3 different states covering simultaneously the frequency bandwidth of one pair of TX and RX sub-channels. This technique will bring some miniaturization by requiring less instantaneous bandwidth than a passive design that would cover the whole band 20([4],[5],[6]).

| Tx1 | Tx2 | Tx3 | | Rx1 | Rx2 | Rx3 |

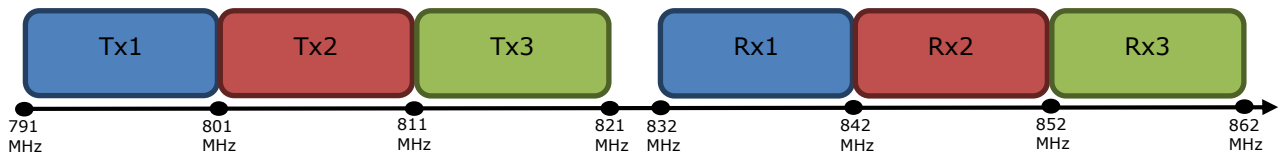791 MHz · 801 MHz · 811 MHz · 821 MHz · 832 MHz · 842 MHz · 852 MHz · 862 MHz

Figure 18   Band 20 channels

In this section, band 20 antenna concept will first be described in its single band passive version. Then the multiband characteristic will be explained and finally, the frequency agility will be introduced and described. This approach will allow the reader to understand what makes the antenna compact, multiband and frequency agile.

- Single band capacitive fed patch

This antenna design comes initially from the antenna family called Monopole Coupled Loop Antenna (MCLA) ([7]). Those antennas work well when placed in the middle of a flat ground plane and have the right radiation properties regarding our requirements. A first single band passive antenna has been designed including a capacitive load as a first miniaturization feature (Figure 19). On one side of the antenna, a capacitive feed can be found (Figure 19(a)). It brings the RF signal to the antenna and the capacitor value controls the matching of the antenna. On the other side of the antenna, a capacitive load can be introduced (Figure 19(b)). The value of its capacitance controls the resonance frequency. This feature miniaturizes the antenna and can be used to introduce some frequency agility.
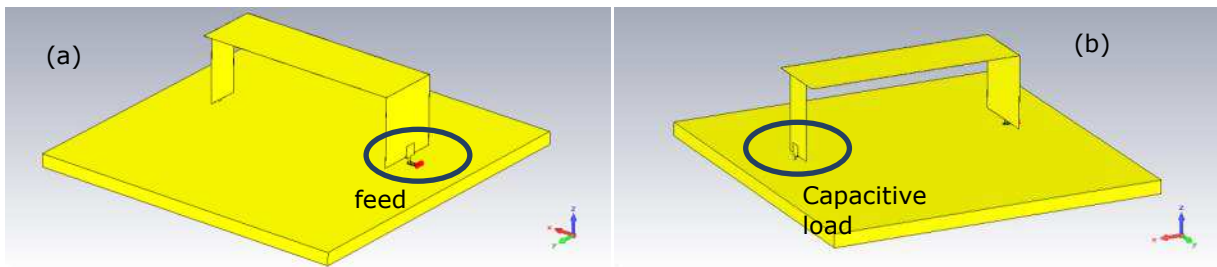
Figure 19   Single resonance antenna
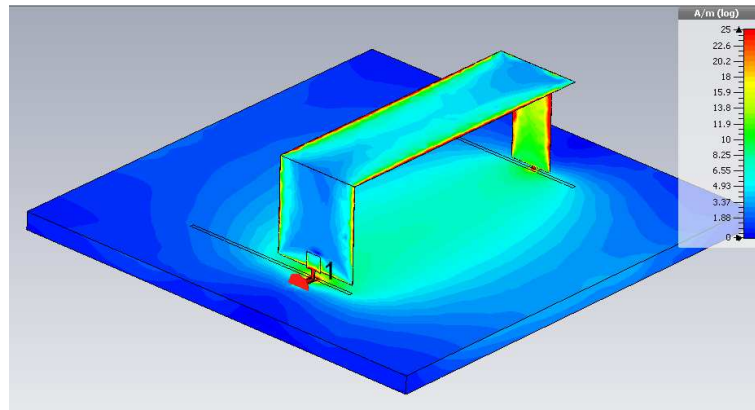

Figure 20   Current distribution
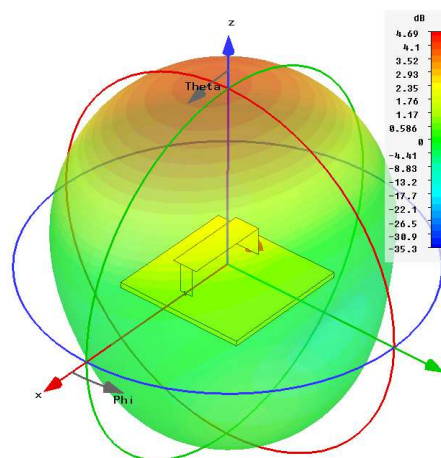
Figure 21   Radiation pattern (realized gain) of the single band antenna

Figure 21 shows the radiation pattern of the single band antenna. Its main beam is towards the Z+ axis and its peak realized gain is 4.7dBi. This antenna has the radiation characteristics specified in the antenna requirements.

- Multiband antenna

In order to generate a second resonance, the top part as well as the end of the strip has been extended and a slot has been added to create two distinct paths for the surface currents and thus two resonances (Figure 22). This phenomenon can be clearly identified by analyzing the surface current repartition at the two specific resonance frequencies (Figure 23).

The dimensions of this antenna are $66*42*23mm^3$($\lambda_0/5,7*\lambda_0/9*\lambda_0/16,5$ with λ_0 = 379mm@791MHz).
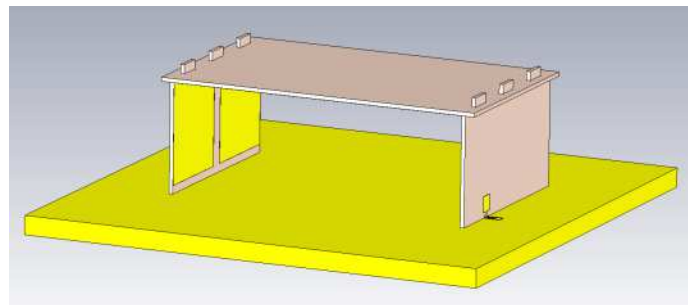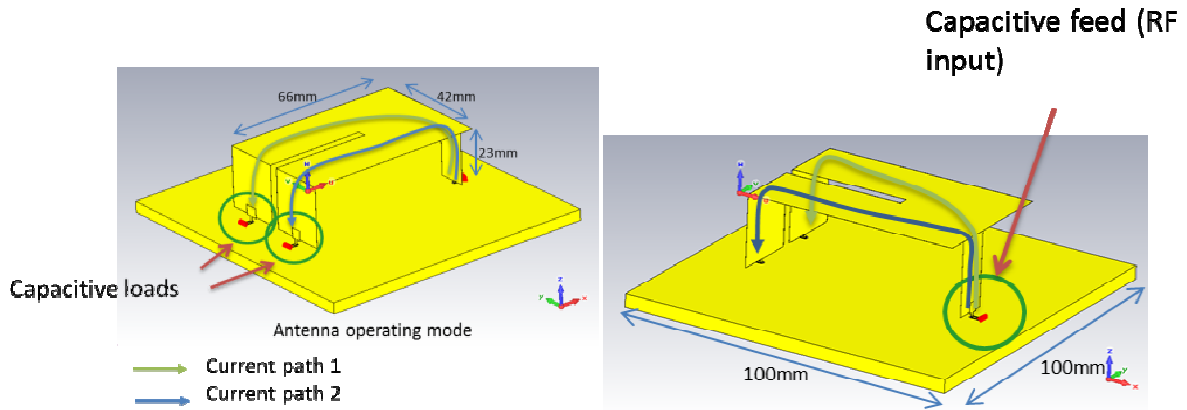
Figure 22   Views of the band 20 antenna

At the end of both paths, a capacitive load has been added (Figure 22) for two reasons. It lowers the resonant frequency and thus miniaturized the antenna but also control the resonance frequency. The frequency agility will be brought through the control of this capacitor value. This will be described later in the document. The control of the capacitance value of those two capacitive loads allows tuning both resonances independently which is clearly an advantage for this antenna topology.

Figure 23   Current distribution

Figure 24   Return loss of the dual band patch antenna

Figure 24shows the reflection coefficient of the compact dual band antenna. The two resonances can be easily identified respectively at 796MHz and at 836MHz. They make the antenna cover two narrow bands of nearly 10MHz bandwidth, 40MHz apart from each other which are the required impedance characteristics for the band 20 antenna.

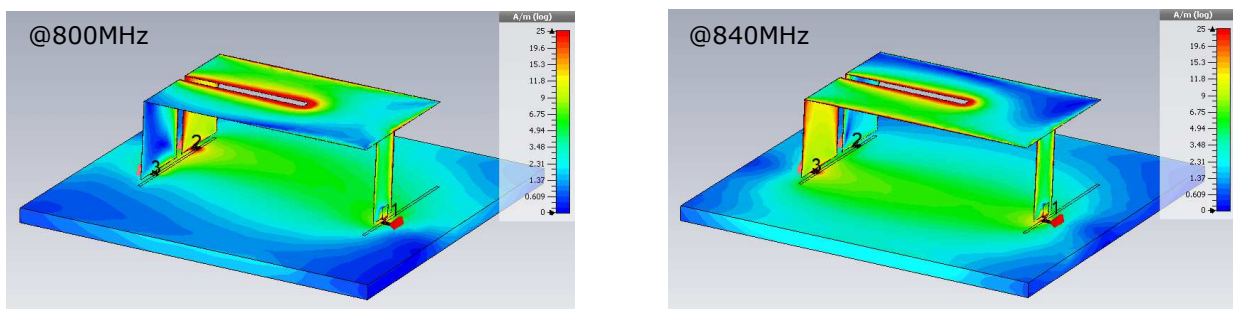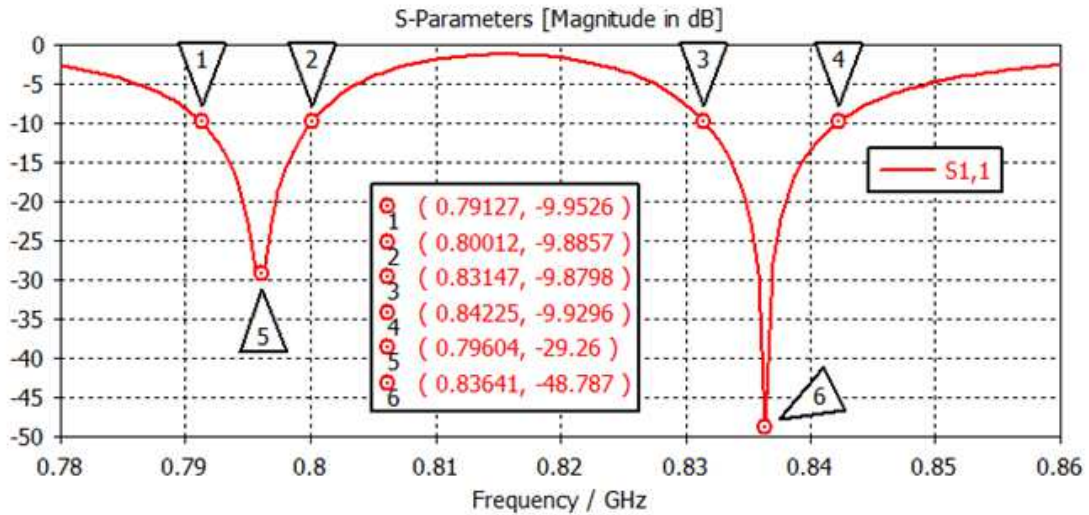For mechanical purpose, the antenna will be printed on a Rogers RO4003 substrate. This technology will ensure a reliable mechanical assembly as well as controlled coupling characteristics for both the capacitive loaders and the capacitive feed. This specific substrate has been chosen for its electrical properties (eg. low dielectric constant and low loss at radiofrequencies).

- Frequency agile antenna

Frequency agility is obtained through the use of two variable capacitors placed in series with the capacitive loaders at both ends of the antenna. We are planning to use two Digital Tunable Capacitors (DTC) from Peregrine (PE6490x series).

The complete DTCs models have been used in the simulation taking into account all the parasitic effects due to packages and lines. The models of those DTCs have been already validated in previous studies. Thus, simulation results should be quite accurate both in terms of impedance and radiation properties.
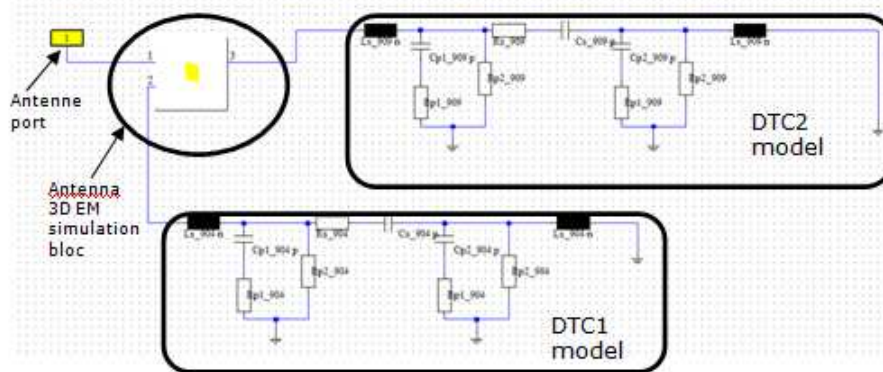
Figure 25   Circuit of the DTCs' model implemented with the CST Studio Suite co-simulation module

A co-simulation (3D EM simulation + RF circuit design) using CST Studio Suite [8] has been performed (Figure 25). The co-simulation provides both impedance and radiation behavior of the antenna system taking into account the losses from both the discrete components (eg. parasitic elements) and the antenna structure itself (eg. dielectric losses).

S-Parameters [Parametric Plot] [Magnitude in dB]

		S1,1 (1)
		S1,1 (2)
		S1,1 (6)

Legend data points:
- 1 (0.79133, -9.9914)
- 2 (0.80011, -9.9708)
- 3 (0.83153, -10.024)
- 4 (0.84222, -9.9371)
- 5 (0.80056, -10.005)
- 6 (0.81047, -10.02)
- 7 (0.8431, -9.9308)
- 8 (0.8531, -10.022)
- 9 (0.81112, -10.055)
- 10 (0.82214, -9.9976)
- 11 (0.854, -9.9896)
- 12 (0.8632, -9.9836)
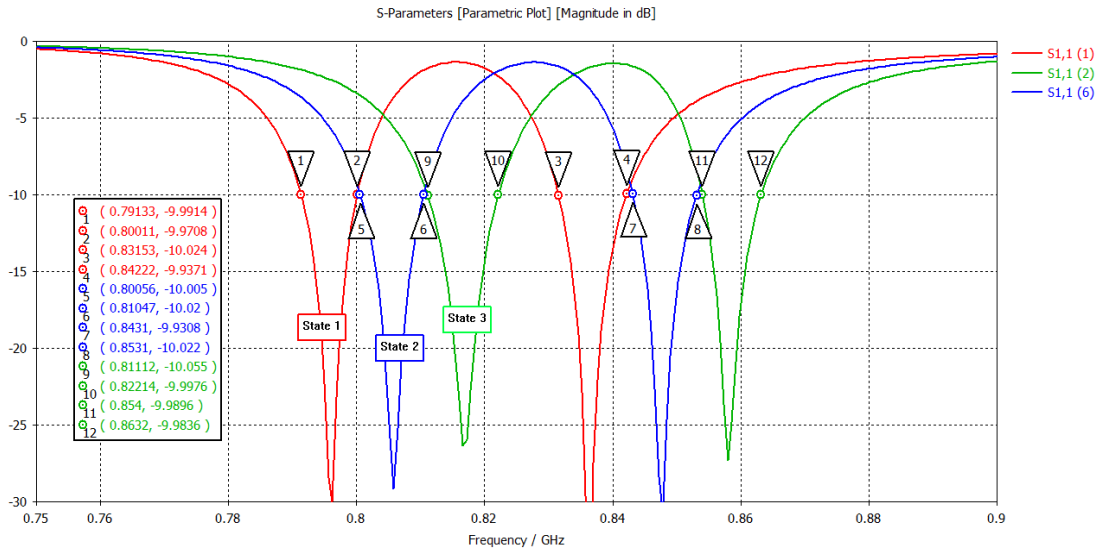
Figure 26   Reflection coefficient of the three states of the antenna

Figure 26shows the reflection coefficient of the band 20 antenna for three different states. Each state has been tuned to cover a specific channel (RX+TX channel) of band 20 as indicated in Table 8. With an instantaneous bandwidth of 20MHz (2x10MHz), frequency agility makes this antenna able to cover the whole band 20 (71MHz) without increasing its volume.

Table 9 Radiation pattern (realized gain) of the stand-alone band 20 antenna

	815 MHz	855 MHz
Phi=0°		
Phi=90°		
3D radiation pattern		

Table 9 shows the radiation pattern (Realized Gain) of band 20 antenna at both resonances for the 3rd state. The antenna has a peak gain of 4 dBi at 815MHz and 4.25dBi at 855M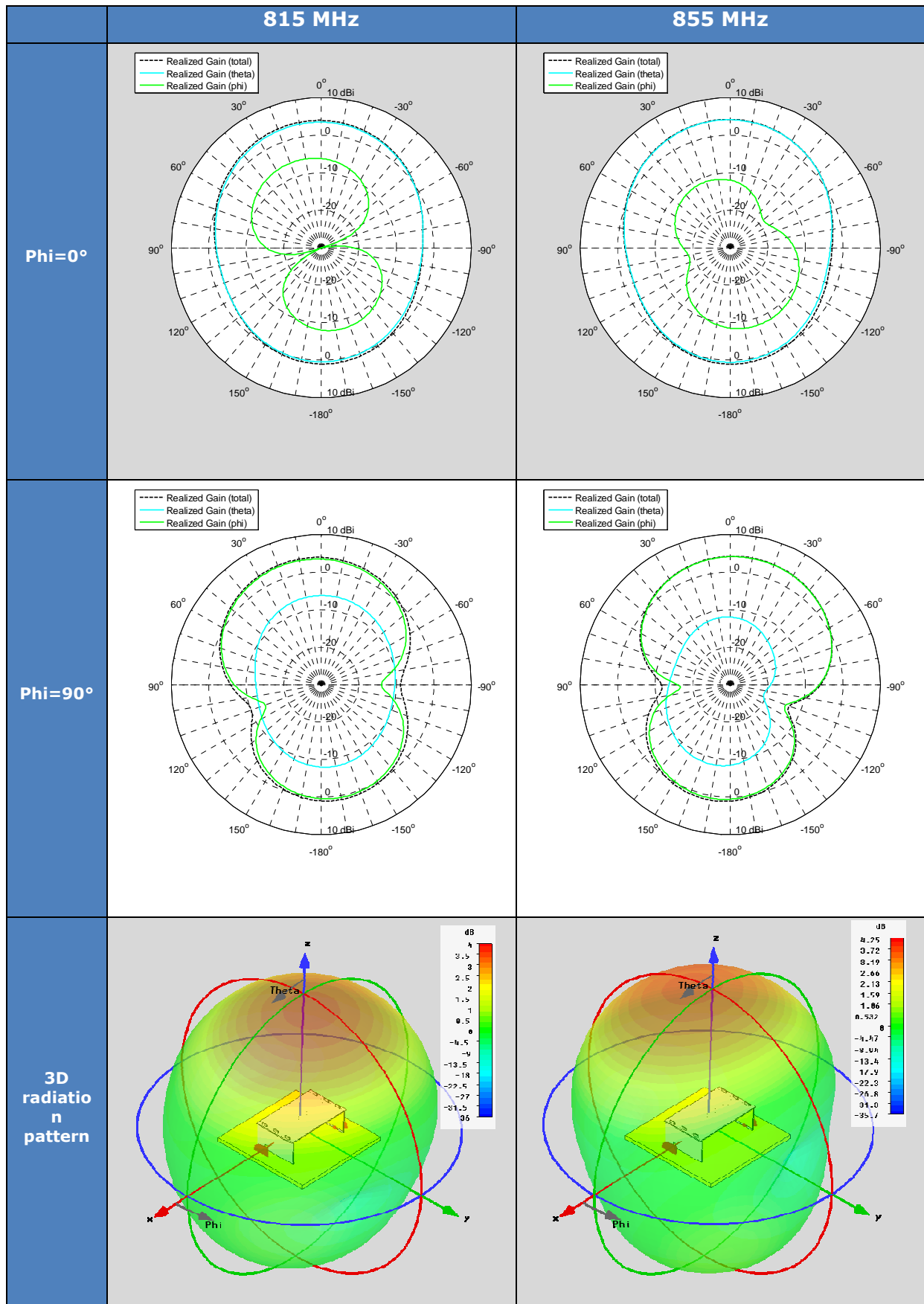Hz. At both frequencies, the peak gain can be found towards the Z+ direction, in line with the antenna requirements. Due to the reduced size of the PCB (ground plane), the front to back ratio is low (around 3dB). This means that there will be some back radiation at those frequencies. The three states of the antenna show the same radiation characteristics.
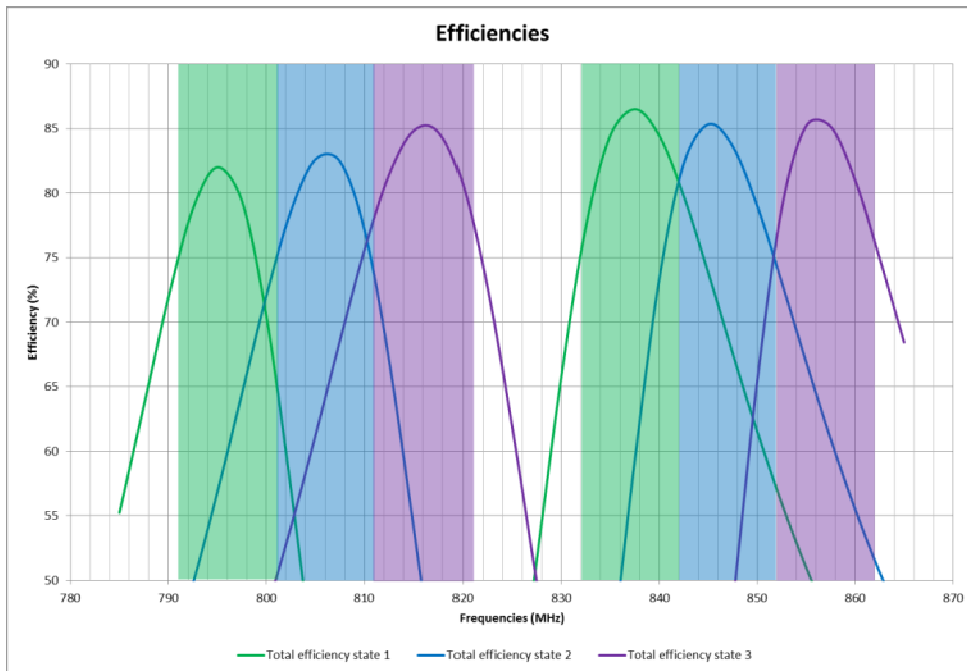
Figure 27   Total efficiency for the different states

The co-simulation results show a total efficiency better than 70% within almost all the band 20 which is very good for a miniature active antenna (Figure 27). Such a good efficiency should provide a very good user experience.

3.2 Band 7 antenna

To cover the LTE band 7, a patch antenna has been designed. This patch covers the whole band 7 (2500MHz-2690MHz).

Band 7 antenna (Figure 28) is a classical patch antenna printed on a 1mm thick FR4 substrate. The size of the patch is 51.5*46mm² and is placed 6mm above the ground plane (λ0/2.3*λ0/2.6*λ0/20 with λ0 = 120mm@2500MHz) to obtain wideband properties. The patch is placed in the center of the ground plane.

Figure 28   Drawings of the band 7 antenna 3D model

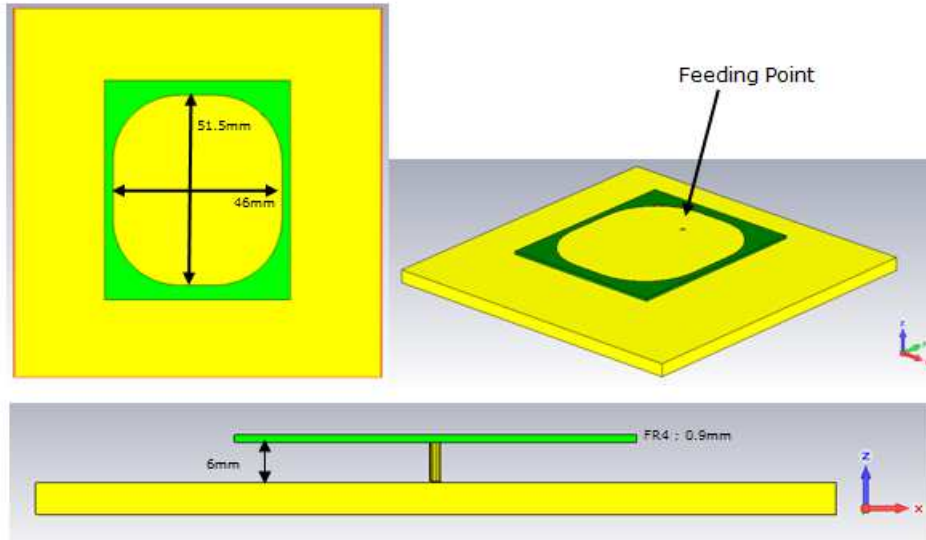The feeding point has been placed so that the patch antenna is well matched to 50Ω and only one mode is excited in order to have the same polarization all over the band 7 frequency range (along the Y axis). The feed is a metal rod (copper) connecting the PCB (RF line) to the main patch (through the FR4 substrate).

For mechanical purpose, 4 nylon spacers will be placed between the main PCB and the band 7 antenna PCB. This will control the distance between the PCB and the antenna as well as the horizontal positioning of the antenna.
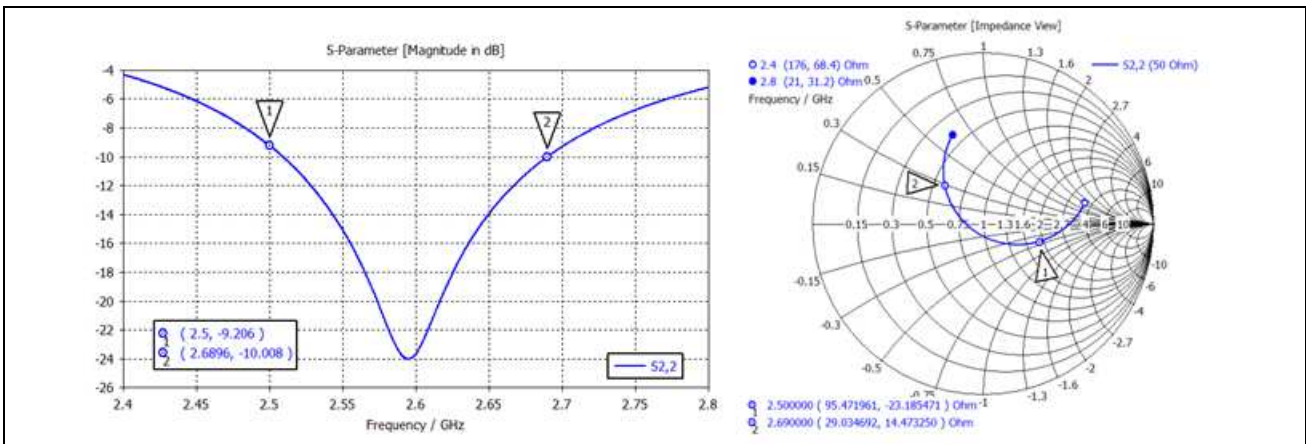
Figure 29   Reflection coefficient and Smith Chart of the stand-alone patch antenna

The patch antenna alone has a return loss below -9dB within the whole band 7 (Figure 29) and it will be easy to reach the -10dB requirement with some fine tuning on the combined antenna prototype. A minimum return loss of -24dB at 2600MHz means almost no mismatch losses at this frequency while a reflection coefficient of -10dB means mismatch losses lower than 0.5dB.
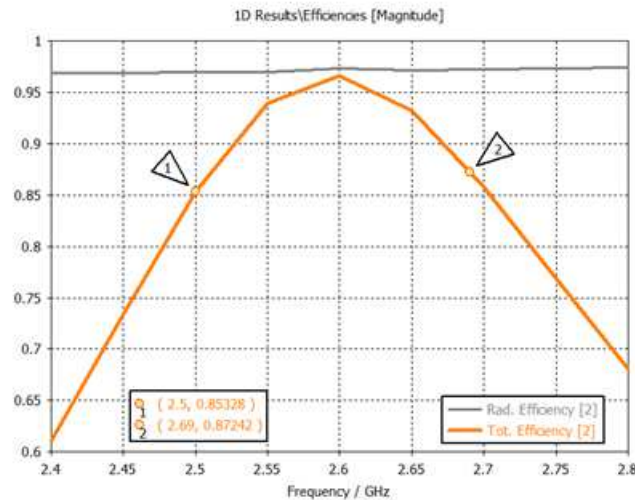
Figure 30   Radiation and total efficiency of the stand-alone patch antenna

The antenna has a total efficiency higher than 85% within the whole band 7 (Figure 30). The radiation efficiency is very close to 100%. This means that the main losses are coming from the mismatch of the antenna impedance.

The radiation pattern (realized gain) matches quite well with the requirement (Figure 31). The main beam is found towards the Z^+ axis and the antenna has a peak realized gain of 8.9dBi. There is almost no radiation towards the Z^- hemisphere meaning a good front to back ratio. At these frequencies, the ground plane presents correct dimensions to fulfill its role.
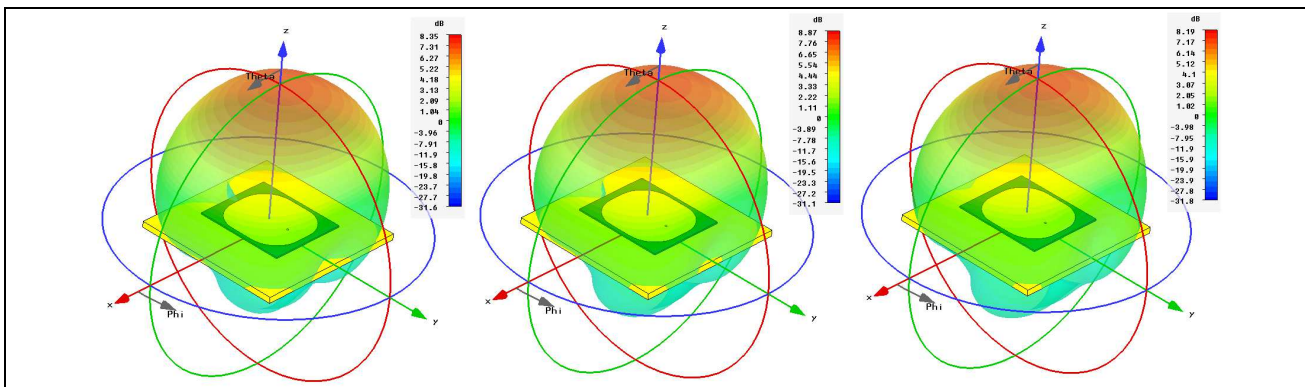
Figure 31   3D radiation patterns (realized gain) (@2500 MHz, 2600 MHz, 2700 MHz)
of the stand-alone patch antenna

3.3 Dual band antenna system for carrier aggregation

The two antennas presented in the previous sections have been implemented together on the same PCB. The difficulties arise from the possible interaction of antenna structures.

The location on the PCB of both antennas has been optimized (Figure 32) in order to reach the best performance of the complete antenna system. They have been placed so that their respective polarizations are orthogonal and thus, the coupling between the antennas is minimized. Also, it has been possible to place band 7 antenna under band 20 antenna. This results in volume optimization as well as radiation pattern stability due to the placement of both antennas in the center of the PCB.

Figure 32   View of the complete 3D model including both antennas

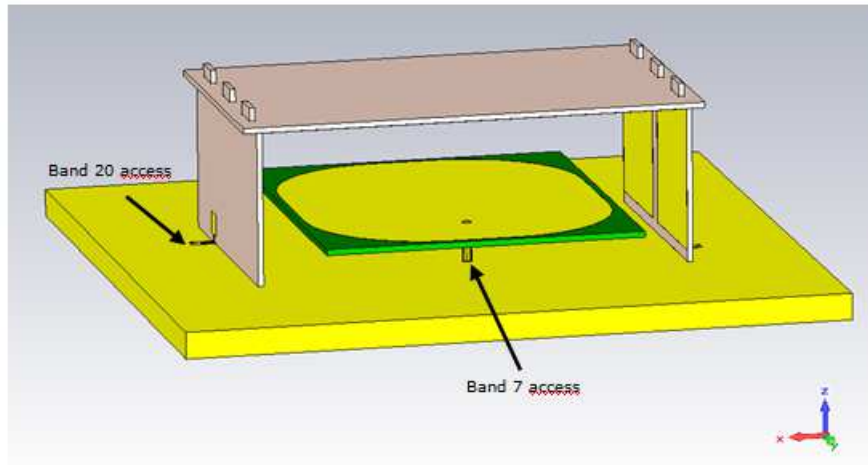In this chapter, the simulation results of the combined solution are presented. These results come from the CST co-simulation including the complete models of the frequency agility active components and the material properties used in the 3D model. As explained previously, this co-simulation setup takes into account all possible losses; thus, the following results should be very accurate and are the ones that will be compared to the measurements planned on the future prototypes.

3.3.1   Integration of both antennas on the same PCB

In order to integrate both antennas on the same PCB an optimization work has been carried out to minimize their impact on each other so that they would keep their own radiation and impedance characteristics. This chapter describes the behavior of the antennas electromagnetic near field whose properties are used to combine both antenna structures while minimizing the interactions between them. The objective is to obtain geometrically nested structures (where the band 20 antenna is somehow hiding the band 7 antenna) that are electromagnetically invisible to each other and keep their main radiation beam towards the Z^+axis.

First of all, the design of each antenna was clearly oriented towards this final combined solution. Thus, they have been designed from the beginning keeping in mind that they should be mechanically compatible.
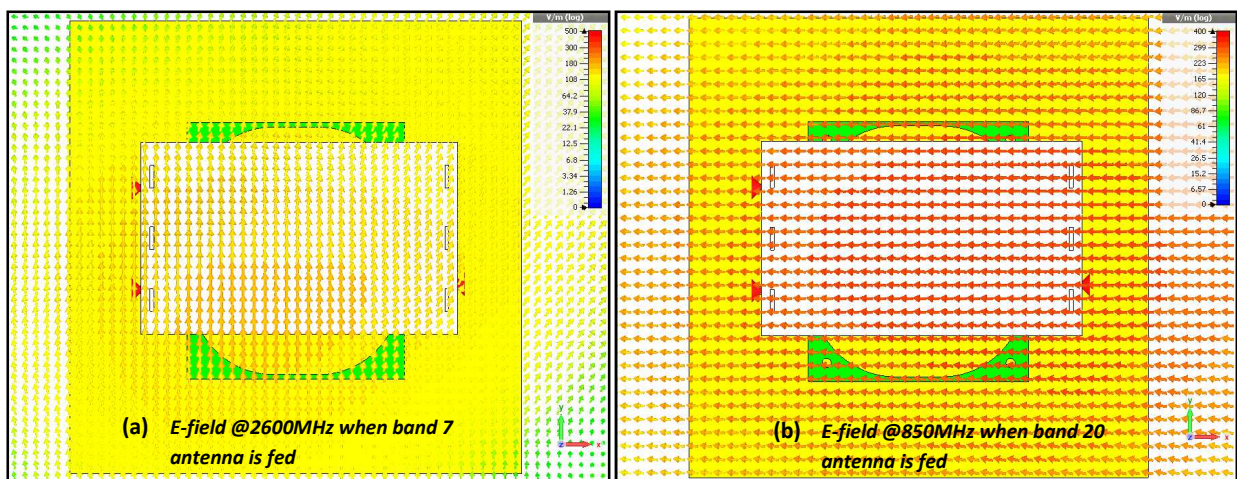
Figure 33   E-field plot on a plane above the antenna system

Figure 33shows the E-field plotted on a plane above both antennas. The orientation of the E-field lines shows that the polarizations of both antennas are orthogonal. Band 7 antenna has its main polarization along the Y-axis while band 20antenna has its main polarization along the X-axis. This configuration is one of the main reasons that explains the relatively low (<-15dB) coupling between both antennas.

Figure 34   E-field plot on a transversal plane of the band 7 antenna along its main
polarization

Figure 34shows the E-field on a transversal plane of band 7 antenna along its main polarization. It can be observed that the E-field magnitude reaches its maximum at both ends of the patch and its minimum in its center. Also, the E-field lines are oriented in an opposite way on both ends of the patch. This behavior is typical of the TM01 resonant mode of a patch. 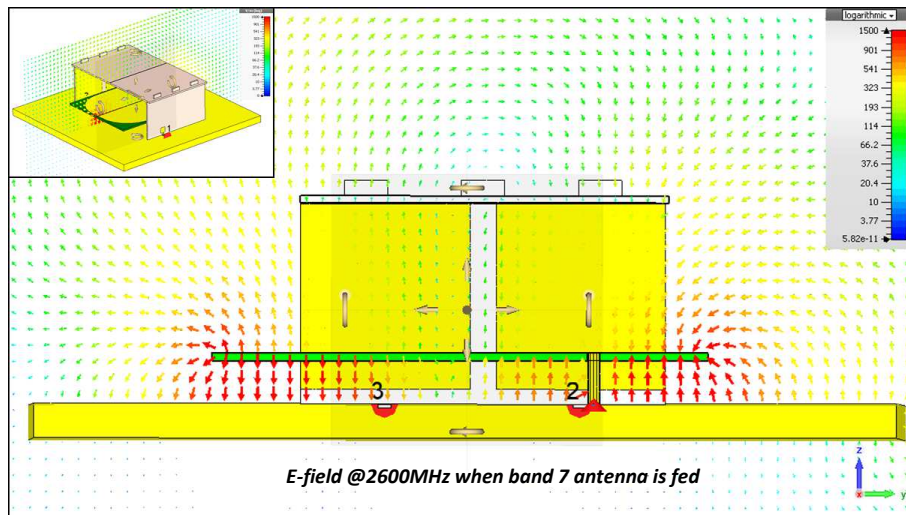This also means that its radiation is mainly generated from its two edges: equivalent two radiating slots model [9]. In consequence, the presence of band 20 antenna right above the center of band 7 antenna doesn't impact the radiation mechanism of band 7 antenna and the radiation of the patch towards the Z^+axis remains possible.
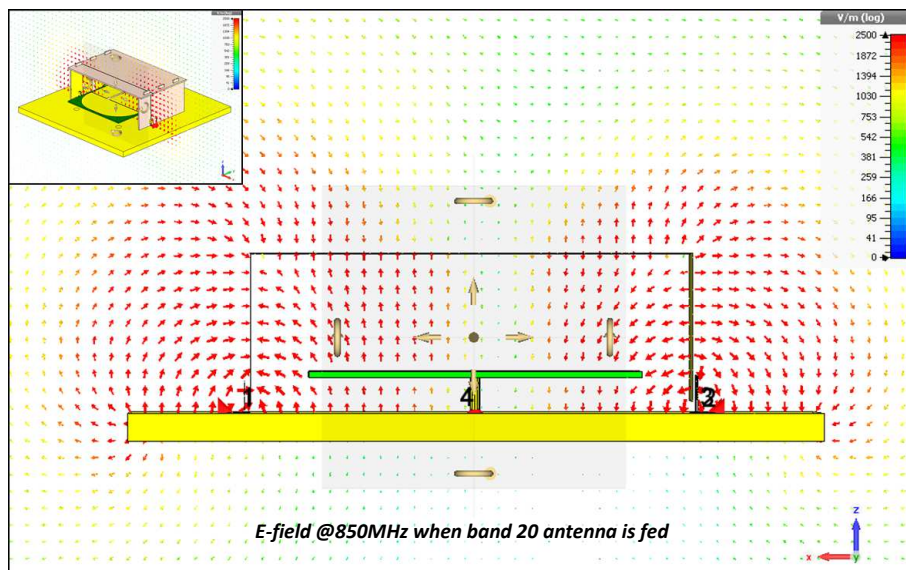

Figure 35   E-field plot on a transversal plane of the band 20 antenna along its main
polarization

Figure 35shows the E-field on a transversal plane of band 20 antenna along its main polarization. We can see that E-field lines have the same behavior as for band 7 antenna. This also means that the radiation comes from both ends of the antenna where the E-field is the strongest.
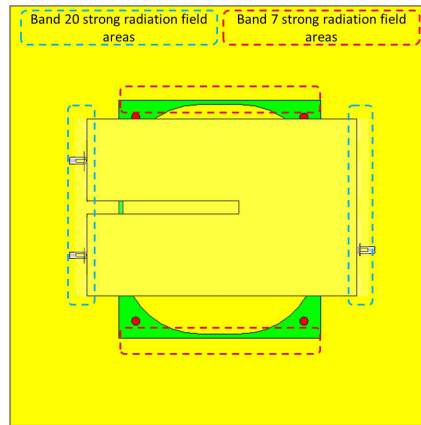
Figure 36   Strong radiation field location of both antennas

The distinct locations of both antennas strong radiation fields (Figure 36) is the second main reason leading to a relatively low coupling (<-15dB) between both antennas. In fact, those radiation areas are located along orthogonal sides and as far as possible from each other taking into account the reduced size of the antenna system.

The coupling figures between both antennas within both frequency bands will be presented in the next section.

3.3.2   Antenna system performance

Figure 37   Reflection coefficient and isolation of the antenna system within the LTE band 20

Figure 37shows the reflection coefficient at the antenna system band 20 access for its three different states. It also shows the isolation between the two antenna accesses within LTE band 20. The simulations show that a reflection coefficient below -9dB (worst case at 862MHz, see Figure 37) is achieved for each state of the antenna, which is very close to the requirement, and will be improved during the final simulation campaign before prototyping phase. Also, isolation (parameters S_{21}) between the two antenna ports better than 15 dB is obtained within the whole band 20 frequency range which exceeds the requirements.

Figure 38   Radiation and total efficiency of the antenna system within the LTE band 20

The simulation shows a total efficiency better than 70% for each band which is very good (Figure 38). Also, it can be observed that the studied combination of both antennas doesn't result in any degradation of the band 20 antenna efficiency.

Table 10   Radiation pattern (realized gain) of the antenna system 3rd state in the LTE band 20

	815 MHz	855 MHz
Phi=0°		
Phi=90°		
3D radiation pattern		
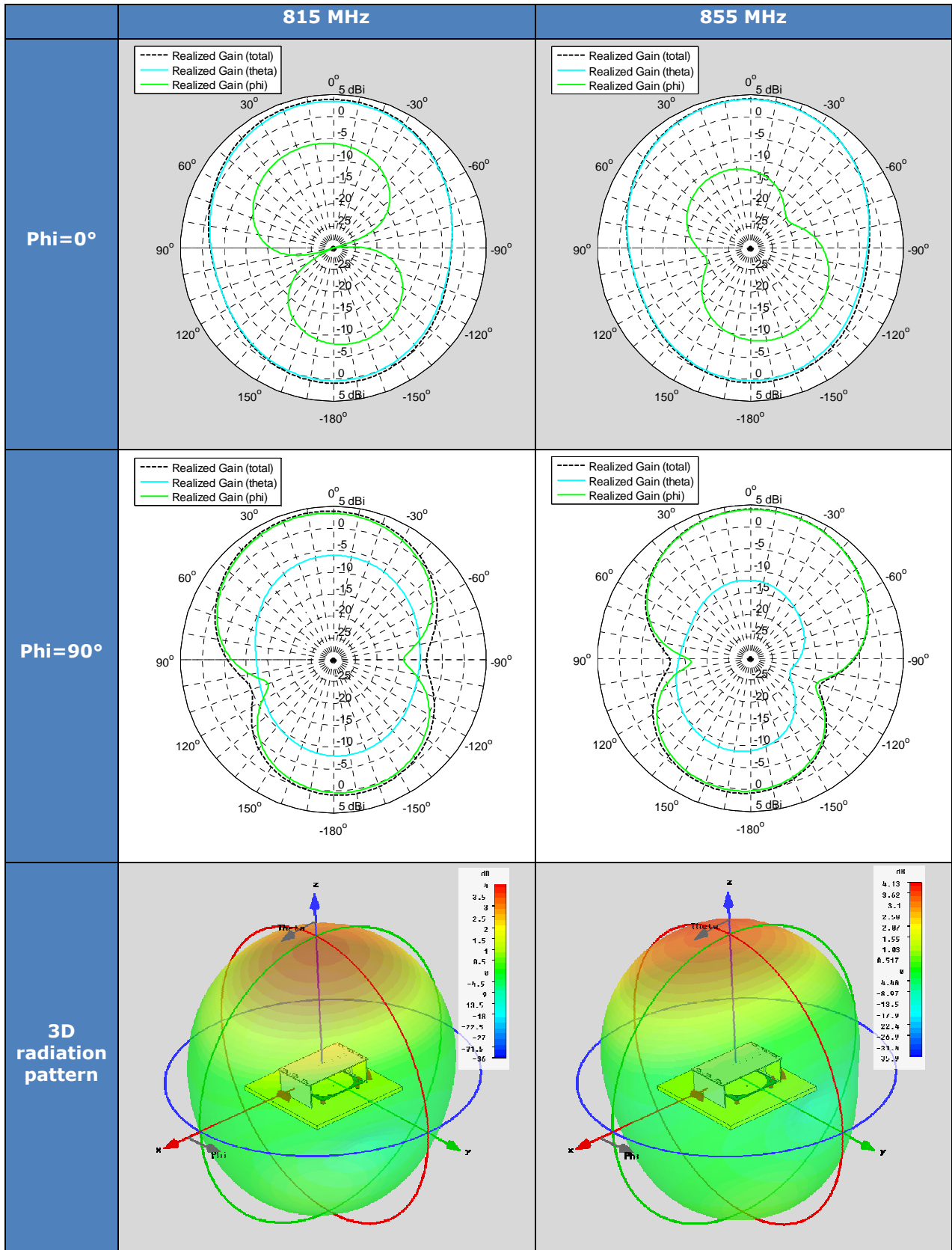
The radiation pattern of the antenna system (Table 10) within band 20 remains very similar to what was observed with the stand-alone band 20 antenna. The main beam remains towards the Z^{+} axis with a peak gain of 4.13dBi.
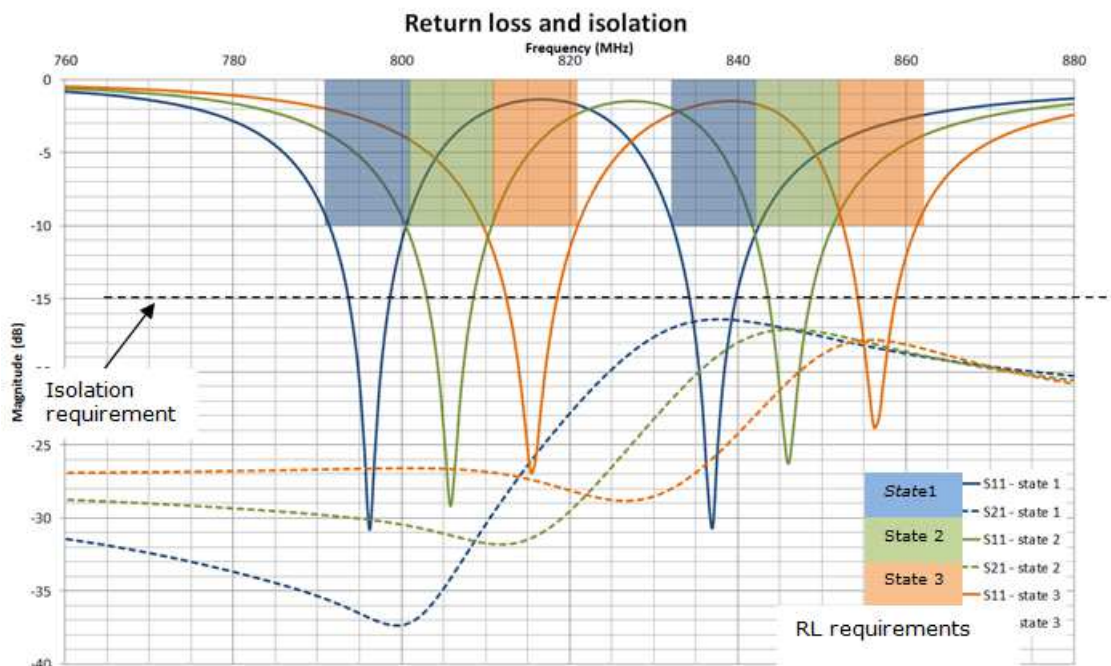
Figure 39   Reflection coefficient and isolation of the antenna system within the LTE band 7

Figure 39shows the reflection coefficient at the antenna system band 7 access for its three different states. It also shows the isolation between the two antenna accesses within LTE band 7. The simulations show that a reflection coefficient below -12dB (worst case) is achieved for each state of the antenna, which exceeds the requirements. Also, an isolation better than 15 dB is obtained within the whole band 7 frequency range, which also exceeds the requirements.
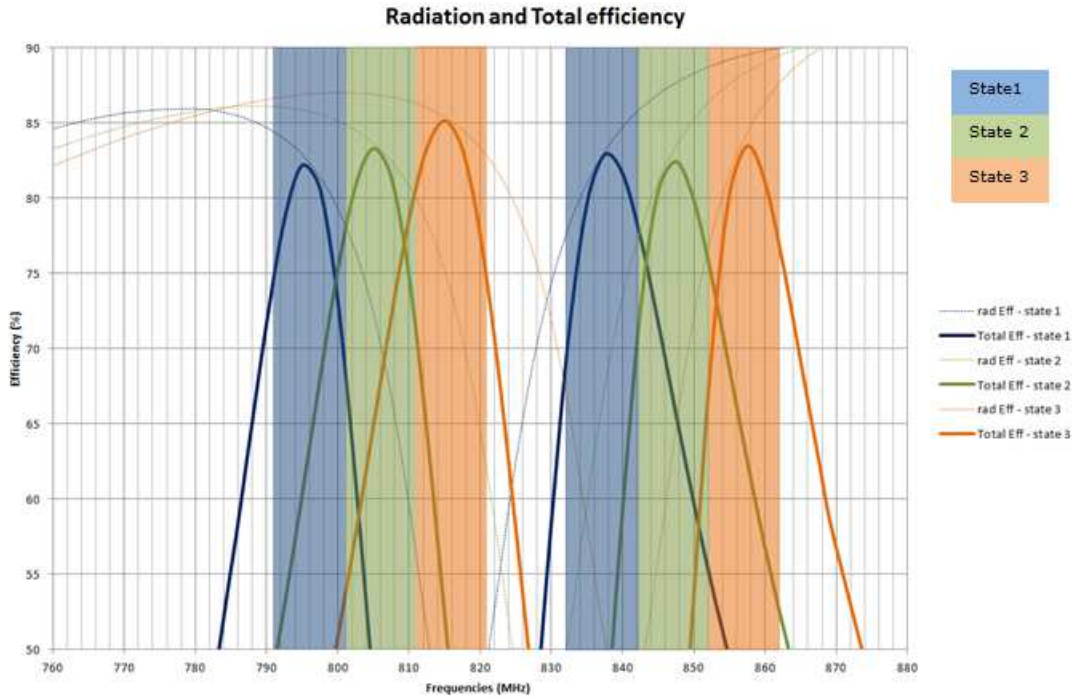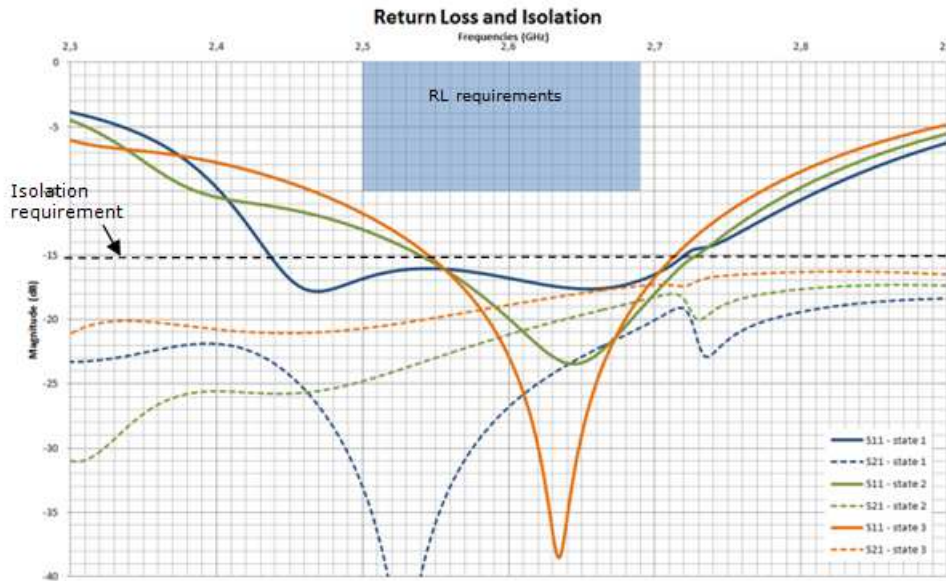

Figure 40   Radiation and total efficiency of the antenna system within the LTE band 7

The simulation shows a total efficiency better than 90% (Figure 40) for each band which is excellent. Also, it can be observed that the studied combination of the two antennas on the same PCB doesn't result in any degradation of the band 7 antenna efficiency.

The radiation pattern of the antenna system within band 7 (Table 11) remains very similar to what was observed with the stand-alone patch. However, it can be observed a slight deviation of the main beam but it still remains very close to the Z^+ axis direction. This small deviation is due to the interaction between both antennas though everything has been done to reduce it as much as possible as explained in the section 3.3.1.

The radiation pattern stays even all over the whole band 7 with the same orientation of the main beam and with a gain variation smaller than 0.5dB.

Table 11   Radiation pattern (Realized Gain) of the antenna system 3rd state in the LTE band 7
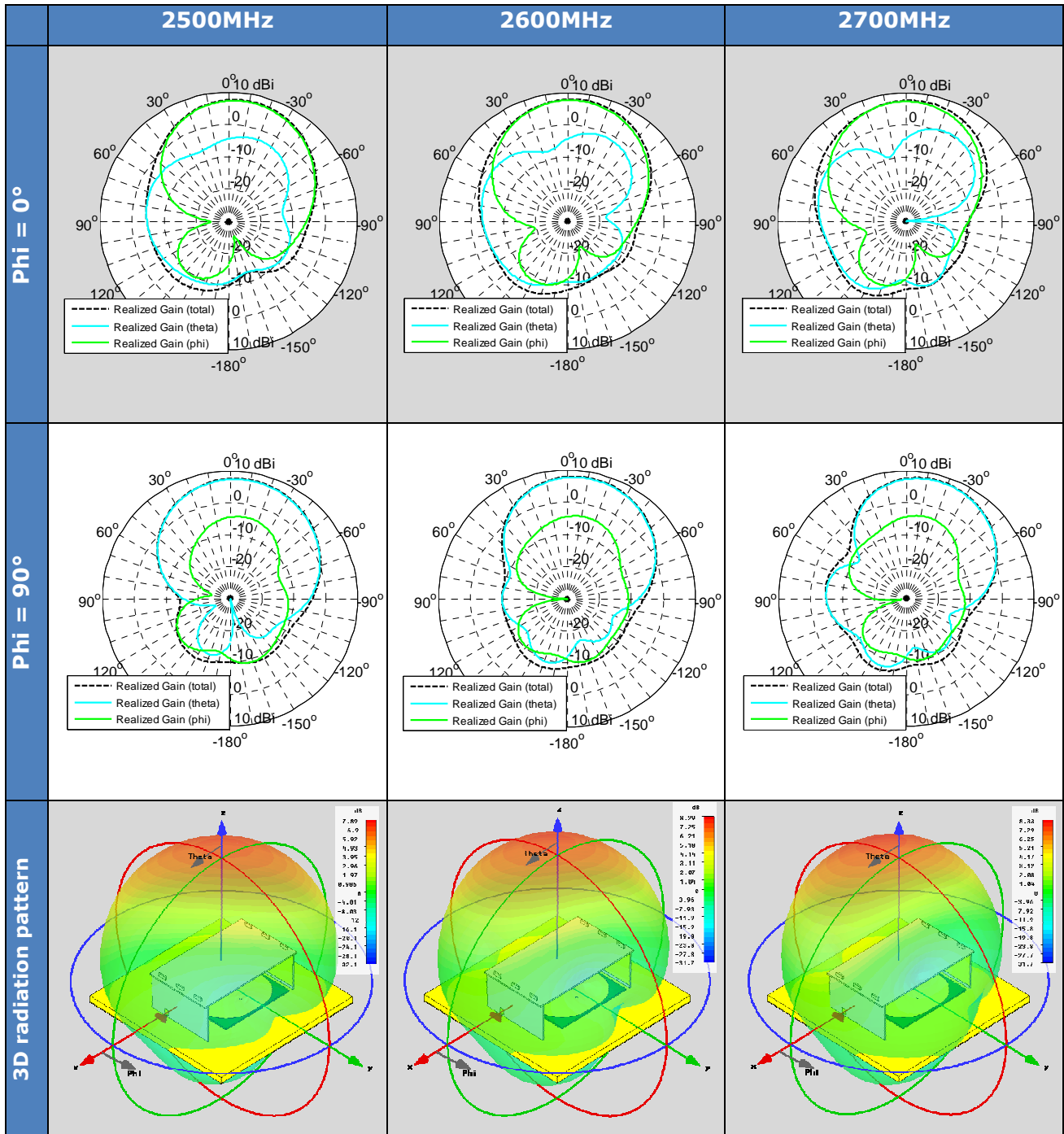
Within the band 7 frequency range, switching from one state to another has an impact on the impedance and the radiation characteristics of the antenna system. However, this impact is neither destructive nor important and thus will not decrease the global performance of the system.

3.4 Conclusion

In this chapter, a complete antenna solution for the small cell base station has been presented. The proposed antenna system fulfils the antenna requirements, is relatively low profile and has a high level of integration. The solution has been optimized regarding the possible CA configurations resulting in a miniaturization of the band 20 antenna thanks to the use of the frequency agility technique.

Passive prototypes of each kind of antenna will be firstly fabricated to individually validate the concepts and associated performance. Then a passive combined prototype will be assembled to confirm the antenna structure combination results. Eventually, an active prototype with both antennas will be realized and measured. This prototype will include all the features presented in this document. The DTC will be controlled through a test board provided by Peregrine. It will validate the simulation results (antenna impedance and radiation behavior) as well as the frequency agility. The use of the DTC will also be validated with this prototype.

An integration work between the RF front-end and the active antenna will be performed. The RF front end will have to control the antenna in order to switch it to the requested state according to its active LTE band and channel configuration.

4   CONCLUSIONS AND THE WAY FORWARD

This document describes the main challenges related to RF front-ends and antennas to support carrier aggregation, which are contained in T3.4 "RF and antenna design" of the SHARING project. Hence, detailed descriptions of the problems and the targeted solutions as well as the challenges related to these solutions are presented, showing some intermediate results.

The purpose of T3.4 is to investigate innovative solutions for RF front-ends and antennas, and to determine to what extent these solutions improve energy efficiency, size or cost in carrier aggregation systems. To this end, the work in T3.4 was divided in two activities: reconfigurable power amplifiers capable to adapt to different CA modes providing energy savings and reconfigurable antennas optimized for the different CA modes allowing size reduction.

Concerning reconfigurable power amplifiers to support carrier aggregation, power amplifier requirements were studied based on CCDF (PAPR) and ACLR evaluation depending on the number of CCs, defining the required output back-off level in each CA configuration. A commercial power amplifier was selected to assess the proposed reconfigurable solution in terms of energy efficiency versus a conventional amplifier. In case of 5 CCs for intra-band contiguous CA, there is not any improvement versus a conventional amplifier. However the evaluation on the commercial PA shows 17.7% relative PAE improvement for 4 CCs, 30.2% for 3 CCs, 45.6% for 2 CCs and 57.9% for single CC. These relative PAE improvement values are related to this specific commercial PA, but they show clearly PAE improvement using different operating points at PA which are optimized for each CA mode.

Antenna requirements have been set according to the available carrier aggregation configurations and the small cell base station application. A complex antenna system using frequency agility has been developed. The whole band 7 and one channel of band 20 is covered by the antenna system instantaneously. Frequency agility has been implemented in band 20 antenna to switch from one channel to another according to the RF front end configuration and thus, make the antenna system able to cover the whole band 20. This technique reduces the instantaneous bandwidth while keeping all the required functionalities and therefore, allows antenna miniaturization. Simulation results shows a reflexion coefficient lower than -10dB all over the required bandwidth. A realized gain better than 8dBi and 4dBi is reached respectively in band 7 and band 20 with in both cases a main beam towards the Z^+ axis.

The information contained in this report about reconfigurable power amplifier requirements for intra-band contiguous CA will be extended to intra-band non-contiguous CA.

Several antenna prototypes will be built and evaluated to validate the antenna simulations. Also, the link between the RF front-end and the antenna command will be made.

REFERENCES

[1] 3GPP TS36.521 Release 12, "User equipment conformance specification radio transmission and reception".

[2] 3GPP TR36.104 Release 12, "Base station (BS) radio transmission and reception"

[3] 3GPP TR36.141 Release 12, "Base station (BS) conformance testing"

[4] H. A.Wheeler, "Fundamental limitations of small antennas," Proc. IRE., vol. 35, pp. 1479-1484, Dec. 1947.

[5] L. J.Chu, "Physical limitations on omni-directional antennas," J. Appl. Phys., vol. 19, pp. 1163-1175, Dec. 1948.

[6] J. S. McLean, "A re-examination of the fundamental limits on the radiation Q of electrically small antennas", IEEE Trans. Antennas Propagat. vol. 44, pp. 672–675, May 1996.

[7] M. Abdallah, L. Le Coq, F. Colombel, G. Le Ray, and M. Himdi, "Frequency tunable monopole coupled loop antenna with broadside radiation pattern," Electron. Lett., vol. 45, pp. 1149–1151, 2009.

[8]   https://www.cst.com/Products/CSTS2

[9] C. A. Balanis, "Modern Antenna Handbook", Chap 4.3.

GLOSSARY

ACRONYM	DEFINITION
3GPP	Third Generation Partnership Project
ACLR	Adjacent Channel Leakage Ratio
BS	Base Station
CA	Carrier Aggregation
CC	Component Carrier
CCDF	Complementary Cumulative Distribution Function
CW	Continuous wave
DC	Direct Current
DL	Downlink
DTC	Digitally Tunable Capacitor
eNB	evolved Node B
E-TM	E-UTRA test model
E-UTRA	Evolved Universal Terrestrial Radio Access
EVM	Error Vector Magnitude
FDD	Frequency Division Duplex
HetNET	Heterogeneous Network
IEEE	Institute of Electrical and Electronics Engineers
IMD3	3 order intermodulation distortion
LTE	Long Term Evolution
LTE-A	Long Term Evolution - Advanced
MCLA	Monopole coupled loop antenna
OBO	Output back-off
OFDM	Orthogonal Frequency Division Multiplexing
PA	Power Amplifier
PAE	Power Added Efficiency
PAPR	Peak to Average Power Ratio
PCB	Printed Circuit Board
RF	Radio Frequency
RX	Reception
SC	Small Cell
SNR	Signal to Noise Ratio
TDD	Time Division Duplex
TX	Transmission

UE	User Equipment
UL	Uplink
WP	Work Package